2016

Impact of Sea-State-Dependent Langmuir Turbulence on the Ocean Response to a Tropical Cyclone

Brandon G. Reichl
University of Rhode Island

Isaac Ginis
University of Rhode Island, iginis@uri.edu

See next page for additional authors

Follow this and additional works at: https://digitalcommons.uri.edu/gsofacpubs

Authors

Brandon G. Reichl, Isaac Ginis, Tetsu Hara, Biju Thomas, Tobias Kukulka, and Dong Wang

Impact of Sea-State-Dependent Langmuir Turbulence on the Ocean Response to a Tropical Cyclone

BRANDON G. REICHL,[a] ISAAC GINIS, TETSU HARA, AND BIJU THOMAS

Graduate School of Oceanography, University of Rhode Island, Narragansett, Rhode Island

TOBIAS KUKULKA AND DONG WANG

College of Earth, Ocean, and Environment, University of Delaware, Newark, Delaware

ABSTRACT

Tropical cyclones are fueled by the air–sea heat flux, which is reduced when the ocean surface cools due to mixed layer deepening and upwelling. Wave-driven Langmuir turbulence can significantly modify these processes. This study investigates the impact of sea-state-dependent Langmuir turbulence on the three-dimensional ocean response to a tropical cyclone in coupled wave–ocean simulations. The Stokes drift is computed from the simulated wave spectrum using the WAVEWATCH III wave model and passed to the three-dimensional Princeton Ocean Model. The Langmuir turbulence impact is included in the vertical mixing of the ocean model by adding the Stokes drift to the shear of the vertical mean current and by including Langmuir turbulence enhancements to the K-profile parameterization (KPP) scheme. Results are assessed by comparing simulations with explicit (sea-state dependent) and implicit (independent of sea state) Langmuir turbulence parameterizations, as well as with turbulence driven by shear alone. The results demonstrate that the sea-state-dependent Langmuir turbulence parameterization significantly modifies the three-dimensional ocean response to a tropical cyclone. This is due to the reduction of upwelling and horizontal advection where the near-surface currents are reduced by Langmuir turbulence. The implicit scheme not only misses the impact of sea-state dependence on the surface cooling, but it also misrepresents the impact of the Langmuir turbulence on the Eulerian advection. This suggests that explicitly resolving the sea-state-dependent Langmuir turbulence will lead to increased accuracy in predicting the ocean response in coupled tropical cyclone–ocean models.

1. Introduction

The energy budget of a tropical cyclone is primarily dictated by air–sea fluxes of heat and momentum (Emanuel 1991). The total heat flux between the ocean and atmosphere under tropical cyclone–force winds is dominated by latent heat flux. Generally, in the warm tropical waters where a hurricane forms, the latent heat flux pumps energy into the atmosphere, occasionally exceeding $1000\,\mathrm{W\,m^{-2}}$ over warm sea surface temperature (SST) during high winds. SST can be greatly reduced under a tropical cyclone due to rapid mixed layer deepening due to vertical mixing and upwelling of cold, subthermocline waters in the presence of horizontally divergent currents. Then, the air–sea heat flux and the energy available to the storm can be significantly reduced (see Price 1981; Emanuel 1999; Bender and Ginis 2000; Ginis 2002). For typical tropical cyclone atmospheric conditions, the latent heat flux can be reduced by an order of magnitude if SST cools by only a few degrees, because the relative humidity of the fully saturated air adjacent to the air–sea interface significantly decreases as the SST cools. It is, therefore, vitally important to accurately model the upper-ocean response to a tropical cyclone and the resulting SST cooling for accurate forecasts of hurricane wind structure, wind intensity, and storm track.

The ocean surface temperature under a tropical cyclone is controlled by both one-dimensional (vertical

---

[a] Current affiliation: Atmospheric and Oceanic Sciences Program, Princeton University, and NOAA/Geophysical Fluid Dynamics Laboratory, Princeton, New Jersey.

Corresponding author address: B. G. Reichl, Atmospheric and Oceanic Sciences Program, Princeton University, 300 Forrestal Rd., Princeton, NJ 08540-6654.
E-mail: breichl@my.uri.edu

mixing/diffusion) and three-dimensional (upwelling and horizontal advection) processes, with each process dominating in certain locations relative to the storm center and for certain storm characteristics (such as size, intensity, and forward translation speed). The one-dimensional process is dominated by the shear-driven vertical mixing of cold, subthermocline water into the mixed layer, which is achieved when turbulent instabilities of the mean current shear overcomes the stable density gradient associated with the thermocline. The cooling due to large-scale three-dimensional processes can become important under tropical cyclones due to the strong spatial variability of the surface forcing (i.e., Yablonsky and Ginis 2009; Vincent et al. 2012). Vertical advection, or upwelling, is a prominent feature of a slowly moving tropical cyclone where horizontal current divergence drives a vertical current that advects subthermocline water into the near-surface mixed layer. Horizontal fluxes of heat are also an important mechanism, particularly near the cold wake associated with a tropical cyclone, because cool water can be advected outward by the cyclonic, wind-driven currents and redistribute heat (Vincent et al. 2012). The effects of upwelling and horizontal advection are not as important when the translation speed of the storm becomes too fast ($>\sim 5\,\mathrm{m\,s^{-1}}$) for three-dimensional processes to establish (Yablonsky and Ginis 2009).

The vertical turbulent mixing of momentum and scalar quantities such as temperature and salt can be significantly enhanced due to the Langmuir turbulence that is driven by the interaction between the surface waves' Stokes drift and the Eulerian current vorticity. This is often referred to as the Craik–Leibovich (CL) vortex force, originally proposed by Craik and Leibovich (1976). This mechanism enhances the vertical mixing over the entire mixed layer even if the Stokes drift is confined in a relatively thin surface layer, as demonstrated by McWilliams et al. (1997) and many subsequent large-eddy simulation (LES) studies (e.g., Noh et al. 2004; Polton and Belcher 2007; Kukulka et al. 2009). Because the intensity of the Langmuir turbulence depends on the relative importance of the wind forcing and the wave forcing, it strongly depends on the sea state through its surface wave field. Therefore, existing upper-ocean mixing parameterizations without explicit sea-state dependence may introduce significant errors in conditions where the surface wave field is not in equilibrium with local wind forcing (Fan and Griffies 2014; Li et al. 2016). The spatial and temporal variability of the Langmuir turbulence intensity is particularly significant in tropical cyclone conditions because the ocean surface wave field is complex, often dominated by large waves misaligned with local wind (Sullivan et al. 2012; Rabe

et al. 2015). This has led to the development of numerous modifications to existing mixing parameterizations to account for variability of the Langmuir turbulence due to sea states. These include modifications to the Mellor–Yamada scheme (Mellor and Yamada 1982), such as Kantha and Clayson (2004) and Harcourt (2013, 2015), and modifications to the K-profile parameterization (KPP; Large et al. 1994), such as McWilliams and Sullivan (2000), Smyth et al. (2002), McWilliams et al. (2012), and Reichl et al. (2016).

A recent modification to the KPP model by Reichl et al. (2016, hereafter RWHGK) has been developed by matching the performance of KPP to equivalent LES results with identical initial conditions and wind and wave forcing, in a wide range of transient wind and wave conditions under tropical cyclones. The study has confirmed that the intensity of the Langmuir turbulence is correlated with the turbulent Langmuir number that characterizes the significance of the wave forcing relative to the wind forcing, as suggested by previous studies. The study has also demonstrated that the Langmuir turbulence significantly reduces the current magnitude inside the mixed layer due to vigorous momentum mixing. The existing, community-standard KPP parameterization is tuned to include typical Langmuir turbulence effects. Therefore, it is able to predict the typical mixed layer deepening events and SST cooling reasonably well; it does not contain the sea-state dependence of such events. For example, it incorrectly predicts the spatial pattern of SST cooling. In addition, the existing KPP appears to entirely miss the enhanced momentum mixing and current magnitude reduction due to the Langmuir turbulence. As stated previously, these mixed layer currents control the three-dimensional response of the ocean to the hurricane, including the upwelling and the horizontal advection of heat. Therefore, the reduced currents due to the Langmuir turbulence may play a significant role in modifying the SST cooling.

The previous study only investigated the impact of the Langmuir turbulence on the one-dimensional (vertical mixing) response to the tropical cyclone. In this study, we investigate the impact of the sea-state-dependent Langmuir turbulence on the three-dimensional response, particularly on the storm-driven horizontal and vertical advection. We will show that the three-dimensional response to the tropical cyclone is significantly modified due to the reduction of the Eulerian currents near the surface that drive advection and upwelling underneath the hurricane center and along the hurricane track. We achieve this by introducing the newly modified KPP by RWHGK in a three-dimensional ocean model coupled with a surface-wave prediction model. Numerical experiments are conducted

using idealized tropical cyclone wind forcing with varying storm translation speeds. The results are then compared with the experiments using the KPP tuned for shear-only turbulence (no Langmuir turbulence) to clarify the overall impact of the Langmuir turbulence. The results are also compared with the experiments using the standard KPP that includes the typical (average, independent of sea states) Langmuir turbulence effects. This addresses an important practical question of whether the explicit (sea-state dependent) Langmuir turbulence parameterization is necessary to accurately predict the SST cooling under tropical cyclones. In our investigation, we also explore the impact of the Coriolis–Stokes force (CS) on the ocean response to the tropical cyclone. The CS is due to the interaction between the Stokes drift and the planetary vorticity in the water column (Ursell and Deacon 1950; Hasselmann 1970; Polton et al. 2005) and is another mechanism by which the Stokes drift can modify the mean current and possibly the SST cooling. There are other mechanisms by which the waves affect the upper-ocean processes, including the resolved-scale CL vortex force, advections of momentum and scalar by the Stokes drift, as well as the impact of growing/decaying wave fields. However, we seek here an understanding of the Langmuir turbulence and the Stokes–Coriolis force alone, and save the complete wave-coupled system for future studies.

2. Methods

a. Description of models

1) MPIPOM-TC WITH KPP

A two-way coupled ocean and wave model has been implemented for this study. The ocean component is the recently updated Message Passing Interface Princeton Ocean Model for Tropical Cyclones (MPIPOM-TC; Yablonsky et al. 2015a), which is a branch in the hierarchy of the Princeton Ocean Model (POM; Blumberg and Mellor 1987; Mellor 2004). This version of POM utilizes message passing interface capabilities in addition to having both one-dimensional (vertical only) and three-dimensional (vertical and horizontal) run options (Yablonsky and Ginis 2009). In this study, the vertical resolution of the model is increased from the operational version of POM in the Hurricane Weather Research and Forecasting (HWRF) Model (Yablonsky et al. 2015b), which has 23 sigma levels to 60 levels (with a constant ocean depth of 2500 m). A near-surface resolution of 4.5 m is kept constant over the upper 200 m of the water column to better resolve the near-surface boundary layer mixing and the

evolution of the mixing layer depth in the KPP model. The traditional Mellor–Yamada (Mellor and Yamada 1974, 1982) vertical mixing routine of POM has been replaced by a turbulent mixing subroutine based on the KPP model (Large et al. 1994), which is described below.

The standard KPP model solves for the vertical turbulent flux terms as follows:

$$\overline{\mathbf{u}_h'w'} = -K_M(z)\frac{\partial \mathbf{U}_h}{\partial z} + \Gamma_U, \tag{1}$$

$$\overline{\theta'w'} = -K_\theta(z)\frac{\partial \Theta}{\partial z} + \Gamma_\theta, \tag{2}$$

where $\mathbf{U}_h$ is the mean horizontal current, Θ is the mean potential temperature, K_X is the eddy mixing coefficient of heat ($X = \theta$) and momentum ($X = M$), z is the vertical coordinate (positive upward), and $\overline{\mathbf{x}'w'}$ is the covariance of the perturbation component of either the horizontal velocity ($\mathbf{x} = \mathbf{u}_h$) or the temperature ($\mathbf{x} = \theta$) with the perturbation of the vertical velocity w. In this study, we neglect the surface buoyancy flux and the resulting nonlocal Γ terms because the contribution of the surface buoyancy flux to the turbulence is relatively small in a high-wind region of a hurricane. We also assume that K_θ and K_M are equal and simply express them as K hereafter, which is consistent with the original KPP formulation when the surface buoyancy flux is negligible. In the KPP model, the vertical profile of K within the surface mixing layer is parameterized as follows:

$$K(\sigma) = hWG(\sigma), \tag{3}$$

where h is the mixing layer depth, W is the turbulent velocity scale, $G(\sigma)$ is the nondimensional turbulent mixing shape function, and $\sigma = -z/h$. In this study W is approximated as $W = \kappa u_\star$ (where κ is the von Kármán constant and $u_\star$ is the magnitude of the surface friction velocity) and $G(\sigma)$ is approximated as $G(\sigma) = \sigma(1 - \sigma)^2$.

In the KPP model, h is defined as the shallowest depth where the bulk Richardson number exceeds the critical value:

$$\mathrm{Ri}_b(z) = \frac{[B^r - B(z)]|z|}{[U^r - U(z)]^2 + [V^r - V(z)]^2 + V_t^2(z)} < \mathrm{Ri}_c, \tag{4}$$

where B is the buoyancy, U and V are the horizontal components of the mean current, and V_t is the unresolved turbulent shear contribution. In this study, the reference values (superscript r) are defined as averages

over the upper 10% of the mixing layer. The unresolved turbulent shear contribution is solved for as follows:

$$V_t^2(z) = \frac{C_v(-\beta_T)^{1/2}}{\text{Ri}_c \kappa^2}(c_s \varepsilon)^{-1/2}|z|NW, \quad (5)$$

where N is the stability frequency and the constants are $C_v = 1.6$, $\beta_T = -0.2$, $c_s = 98.96$, and $\varepsilon = 0.1$ following Large et al. (1994).

We employ three versions of the KPP model in this study. The first, hereafter KPP-ST, is tuned to conditions of shear turbulence only (no Langmuir turbulence). The second, hereafter KPP-iLT, is tuned to typical ocean conditions (with typical Langmuir turbulence) but includes no explicit sea-state-dependent modifications. The tuning for KPP-ST and KPP-iLT was performed to minimize the difference in SST and surface current between the LES results with and without Langmuir turbulence, respectively, of RWHGK and the one-dimensional simulations. It is known that the critical Richardson number used in KPP is dependent on the vertical resolution of the ocean model due to the interpolation needed to find where the bulk Richardson number crosses the threshold value. Since the vertical resolution of the ocean model in this study is coarser than that used in RWHGK, we have retuned the critical Richardson numbers to 0.27 for KPP-ST and 0.35 for KPP-iLT. The third, KPP-LT, includes explicit sea-state-dependent Langmuir turbulence effects. These three versions have been proposed in RWHGK. In that study the performance of each KPP model was evaluated under a wide range of tropical cyclone wind and wave conditions in the one-dimensional General Ocean Turbulence Model (GOTM; Umlauf et al. 2005) by comparing with equivalent LES simulations with identical mean initial conditions and forcing parameters. The first and second versions are the standard KPP model as described above, but with different critical Richardson numbers.

The development of the third version, KPP-LT, is discussed in detail by RWHGK and is briefly summarized below. This model differs from the KPP-ST model in two ways. First, the KPP-LT model utilizes the Lagrangian current in place of the Eulerian current (where the Lagrangian current is the Eulerian current plus the Stokes drift) in the calculation of the turbulent momentum flux:

$$\overline{\mathbf{u}'_h w'} = -K(z)\frac{\partial \mathbf{U}_L}{\partial z}, \quad (6)$$

and in the calculation of the bulk Richardson number:

$$\text{Ri}_b(z) = \frac{[B^r - B(z)]|z|}{[U_L^r - U_L(z)]^2 + [V_L^r - V_L(z)]^2 + V_t^2(z)} < \text{Ri}_c, \quad (7)$$

where the subscript L is used for the Lagrangian currents.

Second, the KPP-LT model introduces an enhancement factor to the eddy viscosity profile and the unresolved turbulent shear contribution to the bulk Richardson number. The enhancement to the eddy viscosity profile F_{LT} is given by

$$K(\sigma) = hWG(\sigma)F_{\text{LT}}(\sigma), \quad (8)$$

with

$$F_{\text{LT}}(\sigma) = 1 + (F'_{\text{LT}} - 1) \times G(\sigma)/\max[G(\sigma)], \quad (9)$$

$$F'_{\text{LT}} = 1 + \text{La}_{\text{SL}\theta'}^{-1}, \quad \text{La}_{\text{SL}\theta'} \geq 0.8, \quad (10)$$

$$F'_{\text{LT}} = 2.25, \quad \text{La}_{\text{SL}\theta'} \leq 0.8. \quad (11)$$

The enhancement to the unresolved turbulent shear, $F_{\text{LT}}^{V_t}$, is different from the enhancement to the eddy viscosity, and takes the following form:

$$F_{\text{LT}}^{V_t} = 1 + 2.3\text{La}_{\text{SL}\theta'}^{-1/2}. \quad (12)$$

Thus, the bulk Richardson number calculation is now

$$\text{Ri}_b(z) = \frac{[B^r - B(z)]|z|}{[U_L^r - U_L(z)]^2 + [V_L^r - V_L(z)]^2 + V_t^2(z) \times F_{\text{LT}}^{V_t}}. \quad (13)$$

Note that this differs from that reported by RWHGK due to a typo, where the $F_{\text{LT}}^{V_t}$ term was incorrectly expressed as $(F_{\text{LT}}^{V_t})^2$.

The surface layer–averaged turbulent Langmuir number $\text{La}_{\text{SL}\theta'}$ is defined as the square root of the ratio of the friction velocity to the Stokes drift averaged over the surface layer (upper 20% of the mixing layer), corrected for the misalignment between the Stokes drift and the Langmuir turbulence:

$$\text{La}_{\text{SL}\theta'} = \sqrt{\frac{u_*}{\langle|\mathbf{u}_S|\rangle_{\text{SL}}}\frac{1}{\max[\cos(\theta_{\text{Waves}} - \theta_{\text{Lag}}), 10^{-8}]}}, \quad (14)$$

where θ_{Waves} is the direction of the Stokes drift averaged over the surface layer, and the direction of the Langmuir turbulence is approximated by the direction of the Lagrangian shear, θ_{Lag}, averaged over the surface layer following Van Roekel et al. (2012). The definition of the surface layer–averaged turbulent Langmuir number in Harcourt and D'Asaro (2008) takes the surface

layer–averaged Stokes drift relative to the Stokes drift at the base of the mixing layer, which we neglect as in RWHGK.

In the ocean model of this study, the Boussinesq horizontal momentum equation is solved including the surface wave impact:

$$\frac{\partial \mathbf{U}_h}{\partial t} + \left(\mathbf{U}_h \cdot \frac{\partial}{\partial \mathbf{x}_h} + W \frac{\partial}{\partial z}\right)\mathbf{U}_h + \mathbf{f} \times (\mathbf{U}_h + \mathbf{U}_S)$$
$$= -\frac{1}{\rho_0}\frac{\partial P}{\partial \mathbf{x}_h} - \frac{\partial}{\partial z}\left(\nu \frac{\partial \mathbf{U}_h}{\partial z} + \overline{\mathbf{u}_h' w'}\right), \quad (15)$$

where $\mathbf{f}$ is the Coriolis vector $(0, 0, f)$ using the f-plane definition centered at 22.4°N, ρ_0 is the mean density, P is the Reynolds averaged dynamic pressure, ν is the molecular diffusivity, and the instantaneous horizontal ($\mathbf{u}_h$) and vertical (w) current components are decomposed into mean ($\mathbf{U}_h$, W) and perturbation ($\mathbf{u}_h'$ and w') components, respectively. (In the actual MPIPOM-TC implementation, these calculations are performed in a σ-level coordinate system, which is identical to the Cartesian expression given here with the constant bathymetry of this study.) In this equation [Eq. (15)] the Stokes drift ($\mathbf{U}_S$) appears in the Coriolis term (Coriolis–Stokes vortex force). In addition, the KPP vertical momentum flux parameterization is modified by the unresolved component of the CL vortex force (Langmuir turbulence) as described earlier.

Complete momentum equations include the resolved-scale CL vortex force and the Stokes advection in the mean equations (see e.g., McWilliams and Restrepo 1999) and the wave momentum budget term in the momentum flux boundary condition (Fan et al. 2010). In this study we do not aim to account for all wave-dependent modifications, rather we show here that the Langmuir turbulence impact is significant and that it is different in one-dimensional and three-dimensional models under tropical cyclones. The Coriolis–Stokes force exists in the one-dimensional framework and has been included in many of the foundational studies of Langmuir turbulence in the literature (e.g., McWilliams et al. 1997). We, therefore, have also included this term. While other wave terms (i.e., resolved-scale CL vortex force, Stokes advection, momentum flux budget) may have a similar magnitude as the Coriolis–Stokes force, we show here that the Coriolis–Stokes force impact is significantly smaller compared to the Langmuir turbulence impact under tropical cyclone conditions. Therefore, inclusion or exclusion of the Coriolis–Stokes force does not affect our main conclusion regarding the Langmuir turbulence impact. We will also find that the

depth-averaged Eulerian current significantly exceeds the depth-averaged Stokes drift under tropical cyclones, and, therefore, we do not expect neglecting the Stokes drift advection to significantly change our conclusions. Although the investigation of the full wave coupled impacts is certainly desirable, it would require significant ocean model modification in addition to modifying the mixing scheme. Therefore, it is left for future investigation.

The drag coefficient used in this study is identical to that proposed by Sullivan et al. (2012):

$$C_d = \begin{cases} 0.0012, & : |u_{10}| < 11\,\mathrm{m\,s^{-1}} \\ (0.49 + 0.065|u_{10}|) \times 10^{-3}, & :11 \le |u_{10}| \le 20\,\mathrm{m\,s^{-1}} \\ 0.0018, & :20\,\mathrm{m\,s^{-1}} < |u_{10}|. \end{cases}$$
$$(16)$$

We have tested the sensitivity of these experiments to different drag coefficient models. While the overall cooling is obviously affected by the drag coefficient choice, the impact of the Langmuir turbulence (the difference among the three versions of the KPP) remains qualitatively similar.

2) WAVEWATCH III COMPONENT

The wave model component of the coupled system is version 3.14 of the WAVEWATCH III third-generation wind-wave model (Tolman 2009). The wind-input source term of the version 3.14 has been modified, using a reduced, wave-age-dependent drag coefficient, to optimize performance under tropical cyclone conditions as described by Moon et al. (2008) and demonstrated by Fan et al. (2009). The wave spectrum is defined over 40 logarithmically spaced frequencies (with a minimum frequency of 0.0285 Hz) and 48 evenly spaced directions. In the model the Stokes drift is calculated as follows:

$$\mathbf{u}_S(z) = \int_0^{k_{\mathrm{UL}}} \int_0^{2\pi} \Psi(k, \theta) 2\omega \exp(2kz)\mathbf{k}\,d\theta\,dk, \quad (17)$$

where $\Psi(k, \theta)$ is the wavenumber-direction variance spectrum, k is the wavenumber, θ is the wave direction, $\mathbf{k}$ is the wavenumber vector, $\omega = \sqrt{gk}$ is the wave angular frequency, and k_{UL} is the upper bound of the wavenumber integration corresponding to a wavelength of 1 m. The Stokes drift is explicitly integrated and averaged over the model levels for the upper 25 m such that the values at the vertical grid centers used in the ocean model represent the mean Stokes drift over those levels, and it is these values that are then passed to the ocean model. In the ocean model a decay scale based on the mean wavelength is used to extrapolate the Stokes drift

below 25 m. Since the Stokes drift at 25 m is small and is determined by the long wave swell field, this extrapolation is adequately representative of the explicit solution. The surface layer–averaged Stokes drift needed for Eq. (14) is computed separately through explicit integration of the wave spectrum and passed in addition to the ocean model.

In principle many parameters should be passed back and forth in the two-way fully coupled ocean–wave model system. For this study we have disabled the impact of the ocean model on the wave model, using the model as a one-way coupled system. The communication from the wave model to the ocean model is restricted to passing the Stokes drift terms only. In this way, we have simplified the problem to focus on the effect of the Langmuir turbulence on the upper-ocean response under prescribed wind and wave conditions eliminating feedback effects between the two models. We have ignored the effect of the ocean current on the waves, the effect of growing/decaying waves on the momentum flux into the ocean (Fan et al. 2010), as well as all the effects of waves and currents on the atmospheric model (i.e., wind forcing). We save investigation of the fully coupled models for future studies.

b. Experiment design

A large, deep-water computational domain is identically defined for both the ocean and the wave model. The ocean and wave model domains are projected into a curvilinear coordinate system based on Earth's latitude and longitude, and model communication and interpolation is then based on the latitude–longitude grid. Both models are simulated on 1/12° resolution domains. The horizontal domain of both models is much larger than the storm size so that boundary conditions are not relevant at the temporal and spatial scales considered. The model is initialized with a homogenous salinity (35 PSU), such that the density structure is determined entirely by the temperature. The initial temperature profile consists of a 20-m mixed layer of 29.25°C, a layer of constant temperature gradient of $0.1°C\,m^{-1}$ from the base of the mixed layer until 120-m depth, a layer of smooth transition between 120- and 1300-m depth, and a realistic lower ocean temperature (4°C) below 1300 m. Because of the short total simulation time the deep ocean is effectively isolated from the surface. The temperature profile is similar to the Gulf of Mexico Common Water temperature profile of Yablonsky and Ginis (2009).

Idealized tropical cyclone winds based on the Holland wind profile (Holland 1980) are inserted into the domain, and translated at varying speeds from east to west. The maximum wind speed is set to $50\,m\,s^{-1}$ and the radius of maximum wind is set to 50 km. We examine three different translation speeds including the stationary case, the $\sim 2.85\,m\,s^{-1}$ case, and the $\sim 5.7\,m\,s^{-1}$ case. For each case, the storm maximum wind is spun up from $0\,m\,s^{-1}$ to the prescribed maximum wind speed over the initial 24 h to minimize the inertial response due to the sudden onset of winds (particularly for the stationary case). The ocean current is initially at rest, and in the KPP model the initial turbulence structure is determined entirely by the mixing layer depth. We have also explored the sensitivity of our results by varying the initial temperature profile, the radius of maximum wind, and the maximum wind speed, which are briefly discussed later.

3. Results

a. Wind and wave fields

In Fig. 1, the results of the wind stress (top panels), the surface 4.5-m-layer-averaged Stokes drift (middle panels), and the turbulent Langmuir number defined by Eq. (14) (bottom panels) are presented for the $0\,m\,s^{-1}$ (left panels), $2.85\,m\,s^{-1}$ (center panels), and $5.7\,m\,s^{-1}$ (right panels) translating storms. The middle panels also show contours of the mixing layer depth defined in KPP, since the mixing layer depth is utilized to compute the surface layer–averaged Stoke drift and the turbulent Langmuir number. These results are obtained using the KPP-LT including the CS force. Although the mixing layer depth and the turbulent Langmuir number vary depending on the version of the KPP used and the presence/absence of the CS, their spatial patterns remain quite similar (not shown). The stationary storm results are presented 24 h after the initial 24-h spinup (48-h total). The stationary simulation length is capped at 24 h since it is rare for a tropical cyclone to remain stationary for long periods of time in nature. The 2.85 and $5.7\,m\,s^{-1}$ results are simulated for an additional 24 h (72-h total) so that the wave field and current field become quasi steady with respect to the reference frame moving with the storm. The low value of the turbulent Langmuir number on the right of the moving storms can be explained by the larger developed wave field. In the rear of the storm, the secondary minimum in the turbulent Langmuir number corresponds to the shallowing of the mixing layer, which increases the surface layer–averaged Stokes drift.

b. Temperature and current fields

We present the results of the overall temperature and current fields in the absence of surface wave effects (KPP-ST-noCS) in Figs. 2–4. Figure 2 shows the spatial fields of the surface temperature (top panels) and the Eulerian current at 11.25-m depth. (The choice of this particular
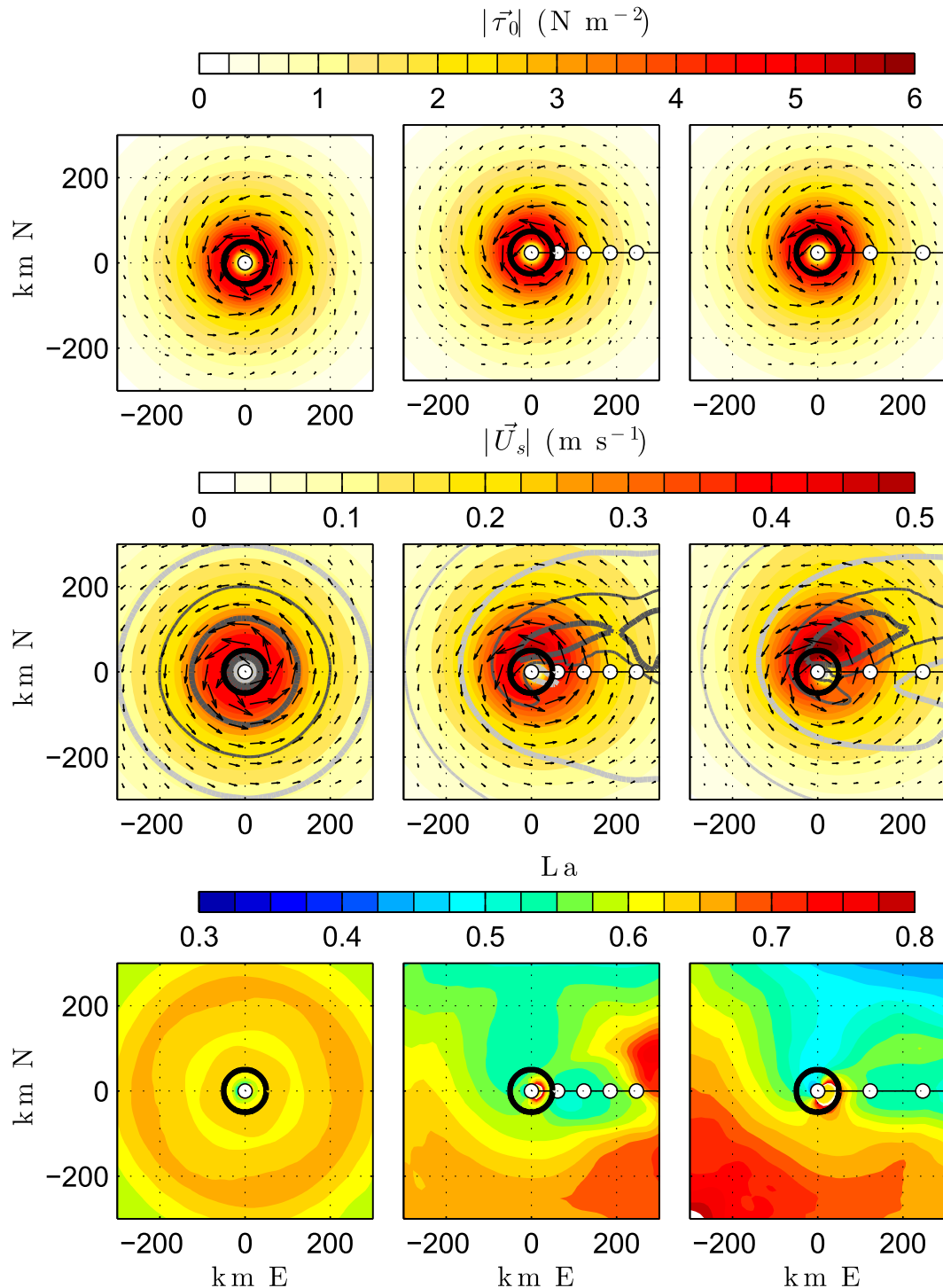
FIG. 1. (top) Wind stress, (middle) surface 4.5-m-layer-averaged Stokes drift, and (bottom) turbulent Langmuir number for (left) a stationary tropical cyclone at 48 h, (center) a tropical cyclone translating at 2.85 m s^{-1} at 72 h, and (right) a tropical cyclone translating at 5.7 m s^{-1} at 72 h, for model runs with explicit Langmuir turbulence and CS (KPP-LT-CS). (top),(middle) The colors indicate magnitude and arrows indicate direction and relative magnitude. (middle) The mixing layer depth contours are also shown at 30 m (thin light-gray contour), 50 m (thick light-gray contour), 70 m (thin dark-gray contour), and 90 m (thick dark-gray contour). The white circles represent the storm center location at 6-h increments and the thick black line is the radius of maximum wind.
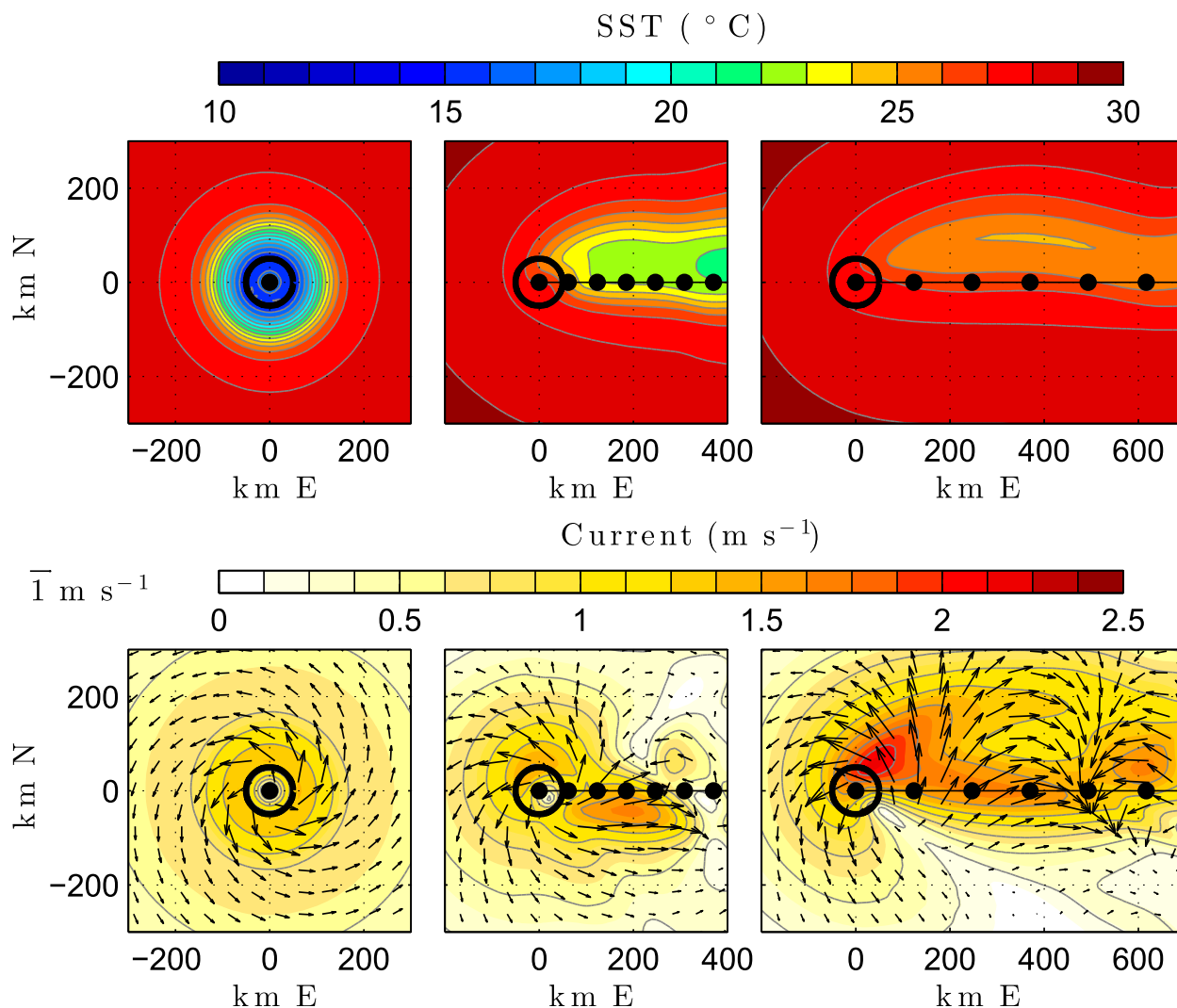
FIG. 2. (top) Mean surface temperature and (bottom) current at 11.25-m depth with KPP-ST-noCS. The black circles represent the storm center location at 6-h increments and the thick black line is the radius of maximum wind. (bottom) The colors indicate magnitude and arrows indicate direction and magnitude. The same three storms are presented as in Fig. 1.

depth is explained later in this subsection.) The vertical transects in the north–south direction at selected locations are shown for the temperature (Fig. 3) and for the current magnitude (Fig. 4). Figure 3 shows that temperature is well mixed and vertically almost uniform inside the mixing layer. In contrast, the current magnitude near the storm center is typically stronger at the surface and decreases with depth. It is more uniform in the rear of the storm (Fig. 4).

The top-left panel of Fig. 2 shows that the temperature is significantly cooled (by over 10°C) near the storm center in the stationary case. This is mainly caused by upwelling due to horizontal current divergence (Fig. 2, bottom-left panel). In nature, such strong cooling is unrealistic because of the feedback effect; the reduced heat flux would rapidly weaken the storm. However, in

our idealized experiment the prescribed wind stress continues to force the upwelling. As the storm translation speed increases, the cooling due to the upwelling effect is reduced, but the cooling due to the mixed layer deepening becomes more important and is stronger on the right of the storm (Fig. 2, top-middle and top-right panels). The rightward bias of cooling appears because the current and the resulting shear-driven turbulence are stronger on the right of the storm due to the resonance effect (Fig. 2, bottom-center and bottom-right panels). The near-surface current, excited by the wind stress, gradually turns to the right (inertial response in the Northern Hemisphere). On the right of the track the wind vector itself also turns to the right (at a fixed location) and continually forces the surface current,
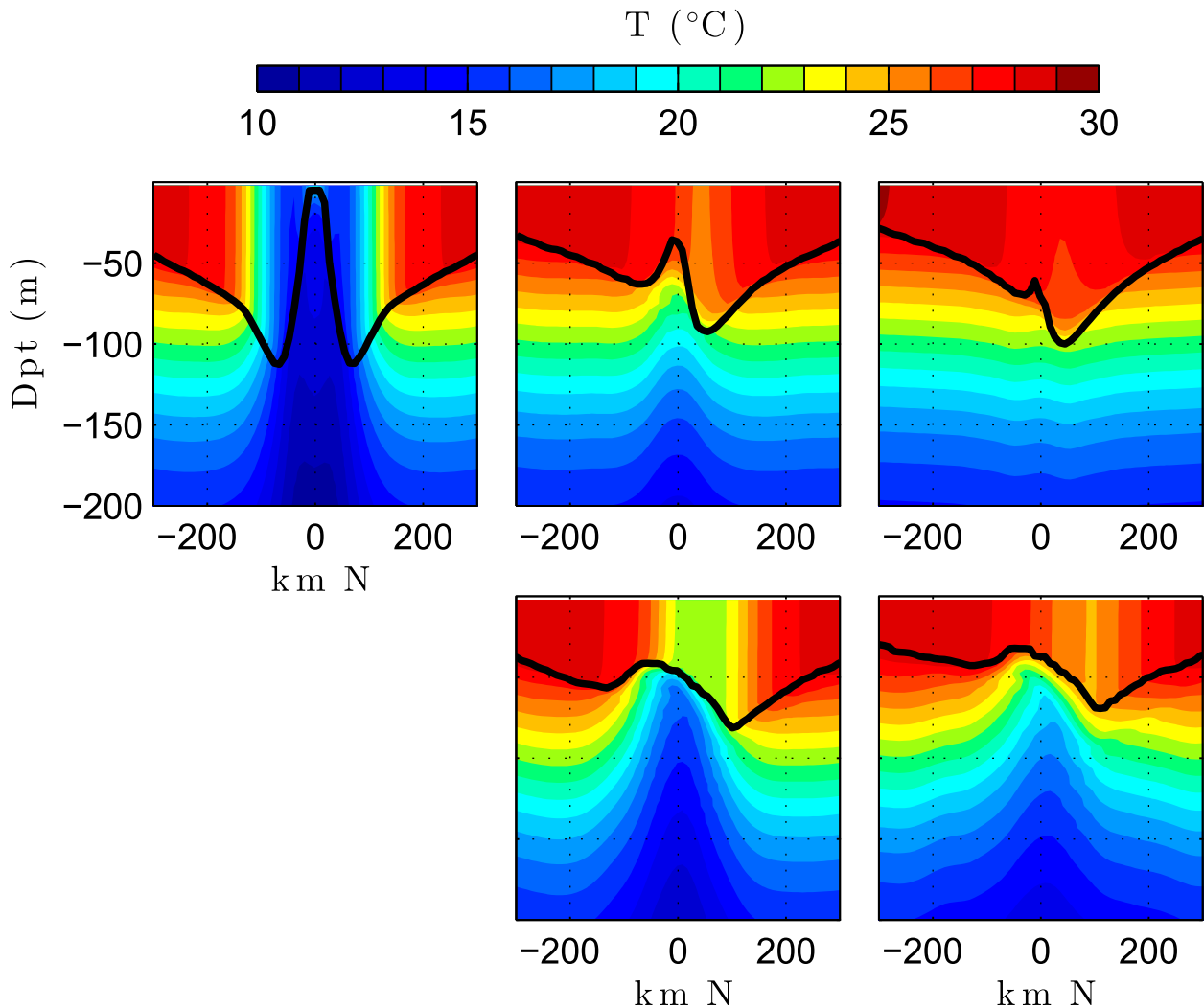
FIG. 3. Vertical transect of temperature in the north–south direction with KPP-ST-noCS. (top) Transects centered at the storm center and (bottom) transects centered at the storm center 18 h prior. The same three storms are presented as in Fig. 1. The thick black line shows the mixing layer depth given by KPP.

causing the rightward bias of the current. For the 2.85 m s^{-1} translating storm, the current magnitude peak on the rear left is caused not only by the resonance process but also by the geostrophic component of the current induced by the pressure gradient associated with the storm upwelling (Ginis 2002). The geostrophic current does not cause enhanced cooling. Indeed, this current peak disappears in the one-dimensional simulation discussed in section 4.

Next we present the results of the overall temperature and current fields with the surface wave effects, that is, with the Langmuir turbulence (KPP-LT) and the CS (this case is denoted KPP-LT-CS) in Figs. 5–7. Although the spatial patterns of the surface temperature and the current (11.25-m depth) in Fig. 5 are qualitatively similar to those in Fig. 2 without the wave effects, the quantitative

difference is significant. The wave effects tend to enhance the surface temperature cooling and weaken the currents. Another striking difference appears in the vertical structure of the current (cf. Figs. 7 and 4). With the surface wave effects the current is more vertically uniform (suggesting enhanced vertical mixing due to the Langmuir turbulence) and does not intensify near the surface. Figure 8 shows the magnitude of the Stokes drift in the same vertical transects as in Fig. 7. Unlike the Eulerian current, the Stokes drift is mostly confined near the surface and becomes insignificant below 10-m depth. The LES results in RWHGK show that the turbulent momentum fluxes are proportional to the Lagrangian shear rather than the Eulerian shear. When there is strong turbulent mixing, the near-surface shear of the Stokes drift introduces an Eulerian current shear that is opposite
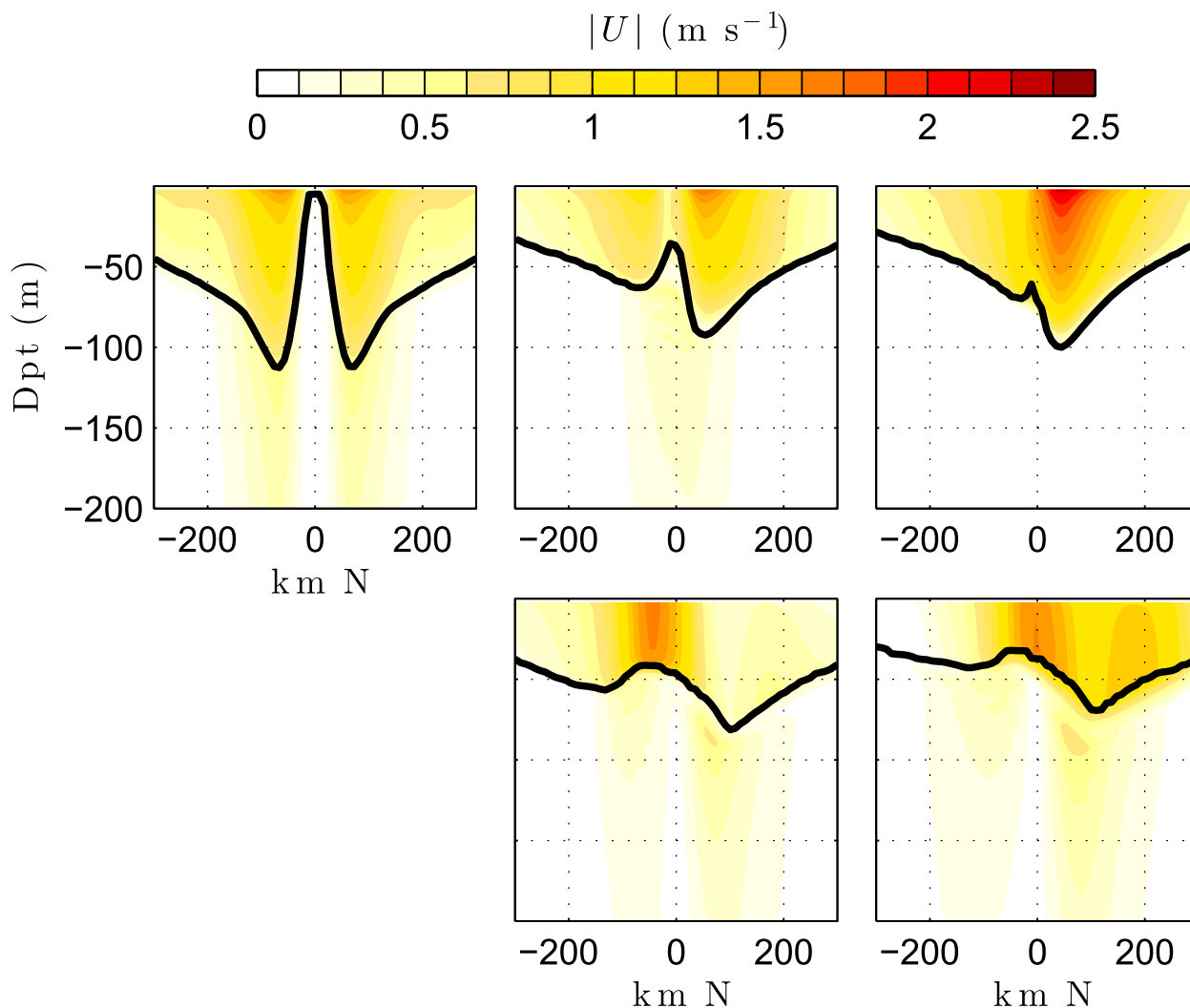
FIG. 4. As in Fig. 3, but for current magnitude.

of the Stokes drift shear (counter-Stokes current) such that the Lagrangian shear is reduced. This tends to decrease the magnitude of the Eulerian current near the surface as seen in Fig. 7. (The Lagrangian current does not decrease near the surface.) Since the Eulerian current is influenced by explicitly including the Stokes drift near the surface, we present the horizontal current fields at 11.25-m depth (below the influence of the Stokes drift) throughout this study. This way, it is clear that the presented differences in the currents are due to the Langmuir turbulence impact, and not due to whether or not we explicitly separate the Eulerian and Lagrangian currents in the model.

In sections 3c and 3d we investigate the impact of the waves in more detail.

c. Impact of Coriolis–Stokes force

Before investigating the effect of Langmuir turbulence, we first address the impact of the CS force.

Figure 9 shows the difference of the surface temperature and the current (11.25-m depth) between KPP-ST-CS (simulation with KPP-ST and with the CS force) and KPP-ST-noCS (simulation with KPP-ST and without the CS force). The color map shows the difference of the temperature and the vectors show the difference of the current. For reference, the isotherms from the KPP-ST-CS results are superimposed on this plot.

For the stationary storm, the temperature at the center is lower in the simulation with the CS force (left panel). This is a consequence of a slight increase of the outward component of the storm-induced current velocity, which increases the current divergence and the associated vertical upwelling of cold water. Since the Stokes drift is nearly cyclonic (in the direction of the wind), the CS force enhances the near-surface outward currents in the early stage. Ultimately in the
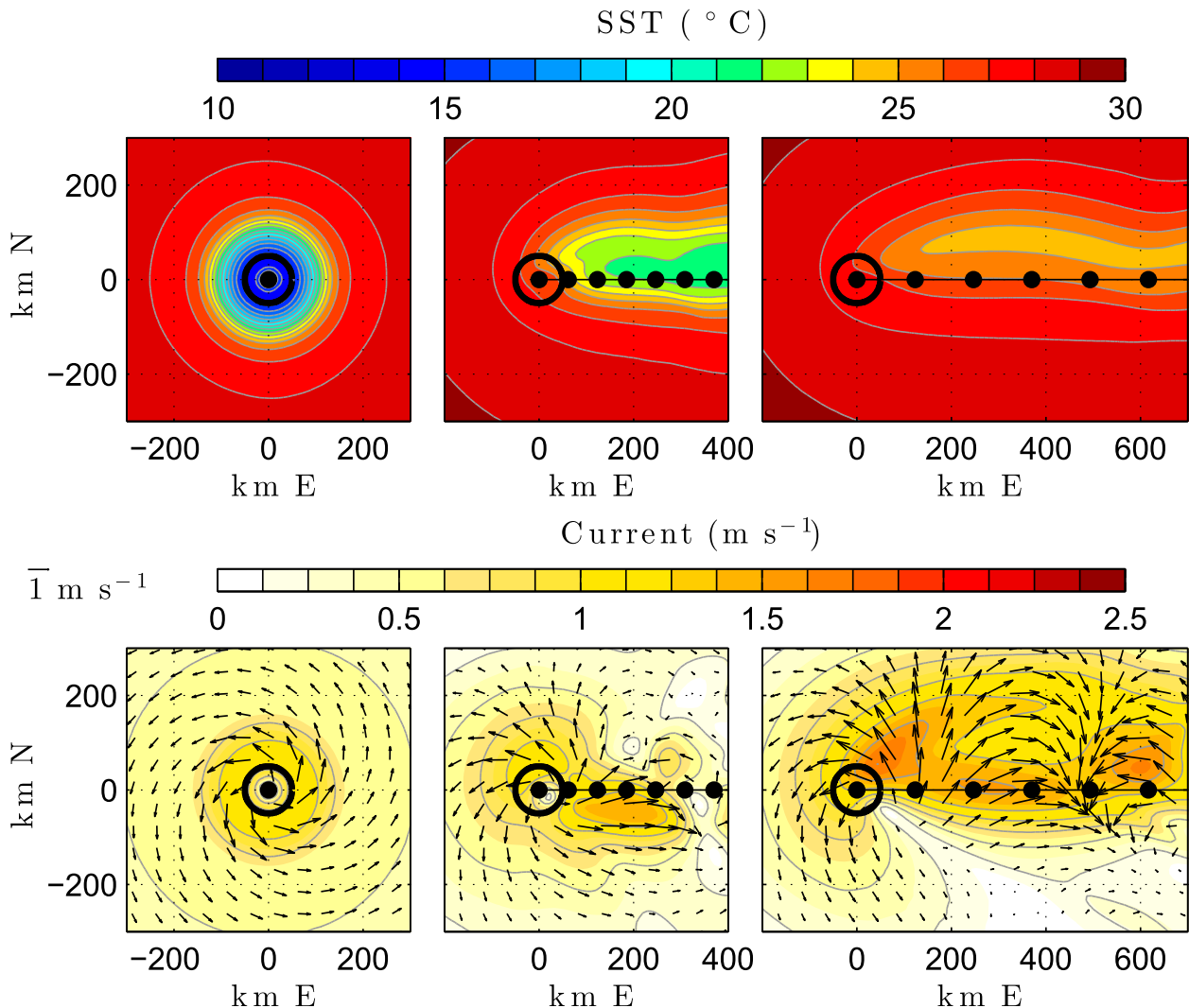
FIG. 5. As in Fig. 2, but for model runs with Coriolis–Stokes force and explicit Langmuir turbulence (KPP-LT-CS).

steady state, this outward force would produce a steady Ekman response and the vertically integrated Ekman transport would be in an anticyclonic direction, exactly canceling the vertically integrated Stokes drift. However, this steady-state solution is not achieved in our 48-h simulation (including 24-h spinup). In fact, such a steady state is unlikely to occur because a tropical cyclone rarely remains stationary for longer than a day in nature.

For the $2.85 \, \mathrm{m \, s^{-1}}$ translating tropical cyclone, there is a warm anomaly to the right rear of the storm's cold wake of up to 0.3°C and a cold anomaly along the left side of the cold wake of up to 0.4°C (middle panel). On the right side of the cold wake, the CS force introduces an excess current across the background isotherms from the warm water to the north toward the cold water in the

wake, which causes the warm anomaly. There is a similar excess current (also due to the CS force) on the left side of the cold wake directed from the cold wake toward the warmer water to the south, which causes the cold anomaly. The cold anomaly on the left is stronger than the warm anomaly on the right because the CS force also increases the cooling due to upwelling (similar to the stationary case, although the enhanced upwelling is much weaker compared to the stationary case). For the faster $5.85 \, \mathrm{m \, s^{-1}}$ translating tropical cyclone (right panel), the upwelling does not have enough time to set up before the storm moves away. There is still a slight warm anomaly on the right and a slight cool anomaly in the rear due to the horizontal advection, though the anomalies are much weaker than those for the slower-moving storm.
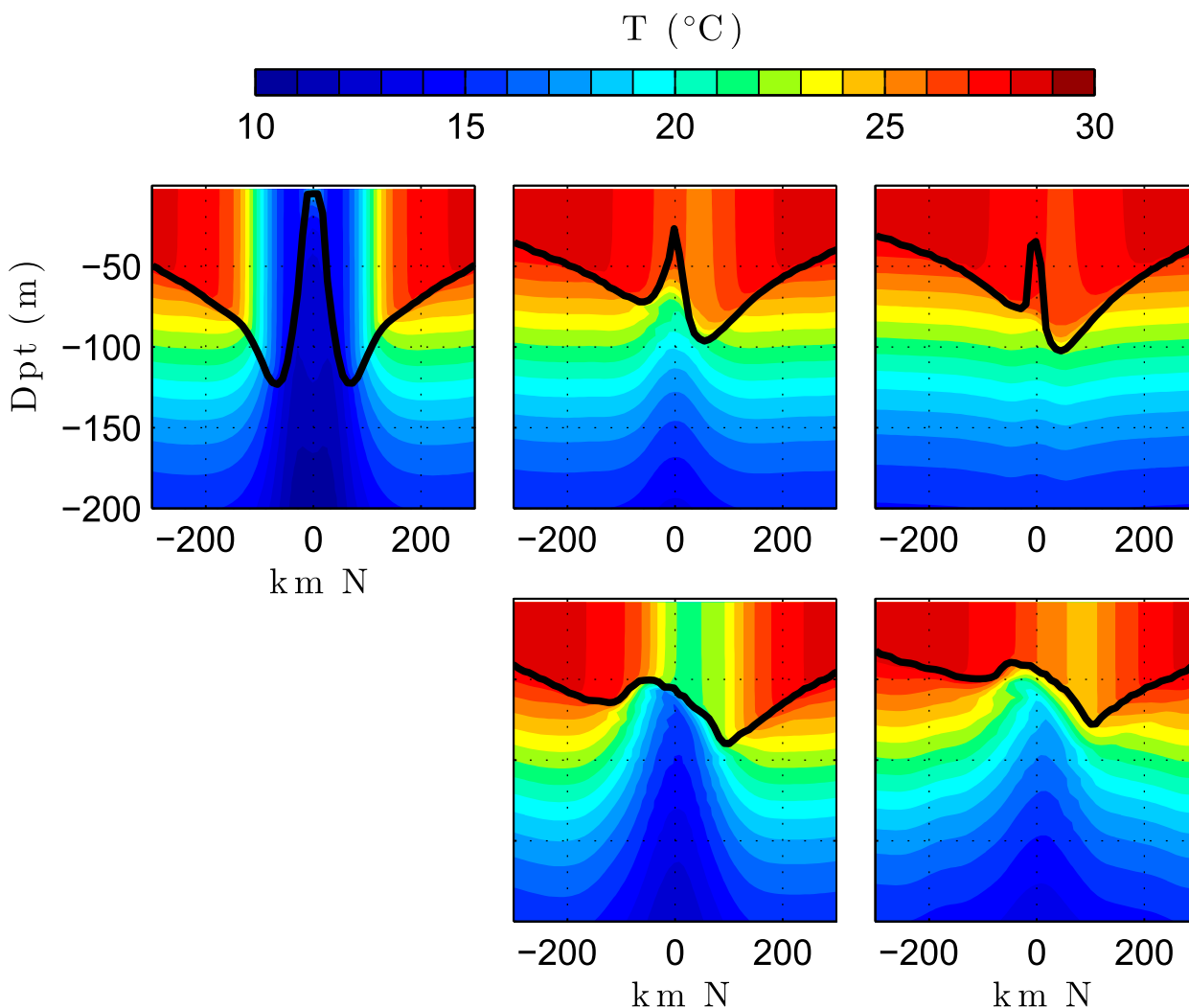
FIG. 6. As in Fig. 3, but with KPP-LT-CS.

In summary, the impacts of the CS force are twofold. First, the CS force increases upwelling due to the divergent current force. This effect is the largest for the stationary storm and rapidly decreases as the storm translation speed increases. Second, for a moving storm the CS force warms the right-hand side of the cold wake and cools the left-hand side of the cold wake due to modified horizontal advection. This effect also weakens as the storm translation speed increases.

d. Impact of Langmuir turbulence

Next, the impacts of the Langmuir turbulence on the near-surface temperature and the currents are investigated. This problem has been previously studied using LES and one-dimensional column models (see Sullivan et al. 2012; Rabe et al. 2015; RWHGK). The impact of Langmuir turbulence on the three-dimensional ocean response, including the impact on horizontal advection and upwelling, has not been investigated prior to this study.

In this subsection the CS force is always included in order to isolate the Langmuir turbulence impact. The top panels of Fig. 10 show the difference of the surface temperature and the current (11.25-m depth) between KPP-LT-CS (simulation with KPP-LT and with the CS force) and KPP-ST-CS (simulation with KPP-ST and with the CS force). The sum of the fields shown in Fig. 9 and the top panels of Fig. 10 is the result of the total wave impact (due to Langmuir turbulence and CS).

The impact of the Langmuir turbulence is significantly stronger than the impact of the CS force. This means that the overall impact of surface waves is predominantly due to the Langmuir turbulence. The Langmuir turbulence enhances surface cooling during
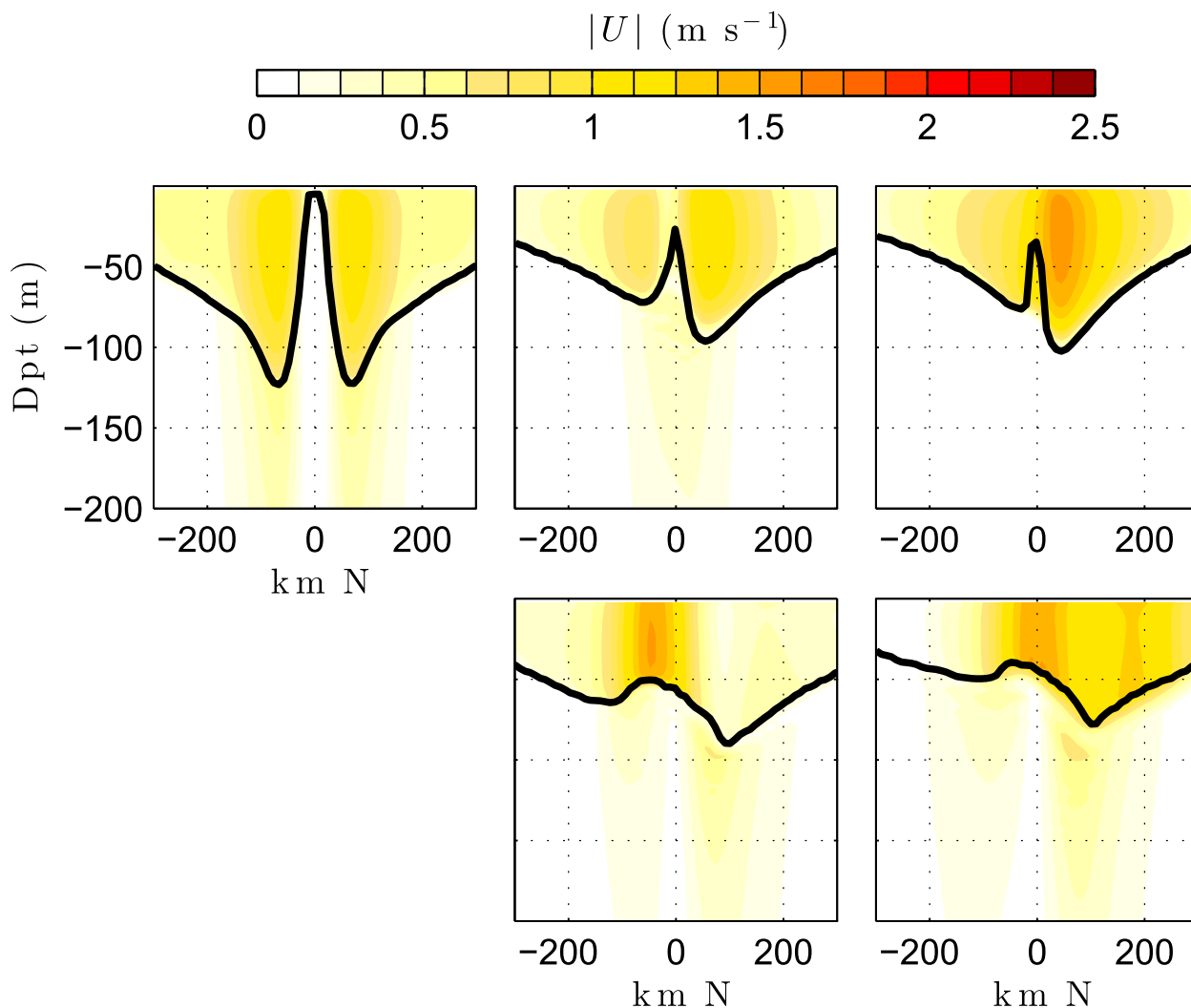
FIG. 7. As in Fig. 6, but for current magnitude.

moving storms by up to 0.7°C, particularly on the left side. For the stationary storm the Langmuir turbulence effect is more subtle, with both warming and cooling occurring at different locations. The vector current difference between KPP-LT-CS and KPP-ST-CS is mostly in the opposite direction of the current vector itself (Fig. 2, bottom panel). This shows that the Langmuir turbulence reduces the current at 11.25-m depth.

To better understand the Langmuir turbulence effect, we carry out two more simulations of KPP-LT-CS-1d and KPP-ST-CS-1d. These two simulations are identical to KPP-LT-CS and KPP-ST-CS, respectively, except that the ocean model is run in one-dimensional mode (without horizontal advection of momentum and heat and gradient of pressure). The difference of the surface temperature between KPP-LT-CS-1d and KPP-ST-CS-1d is shown in the middle panels in Fig. 10. These panels show the impact of the Langmuir

turbulence on the one-dimensional processes only (which is the cooling due to entrainment of cooler water from below the mixed layer).

The Langmuir turbulence enhances the cooling everywhere in the one-dimensional simulation because the surface waves always decrease the turbulent Langmuir number and enhance the vertical mixing compared to the no-wave (shear only) case, which agrees well with the previous studies. One interesting result from the one-dimensional case is that the contribution of the Langmuir turbulence to cooling is larger on the left than on the right for moving tropical cyclones, even though the turbulent Langmuir number tends to be lower (the Langmuir turbulence tends to be stronger) on the right side of the tropical cyclone due to the larger Stokes drift (Fig. 1, bottom panels). This is because the left side of the storm has less shear-driven turbulent mixing, and, therefore, is more sensitive to the Langmuir turbulence.
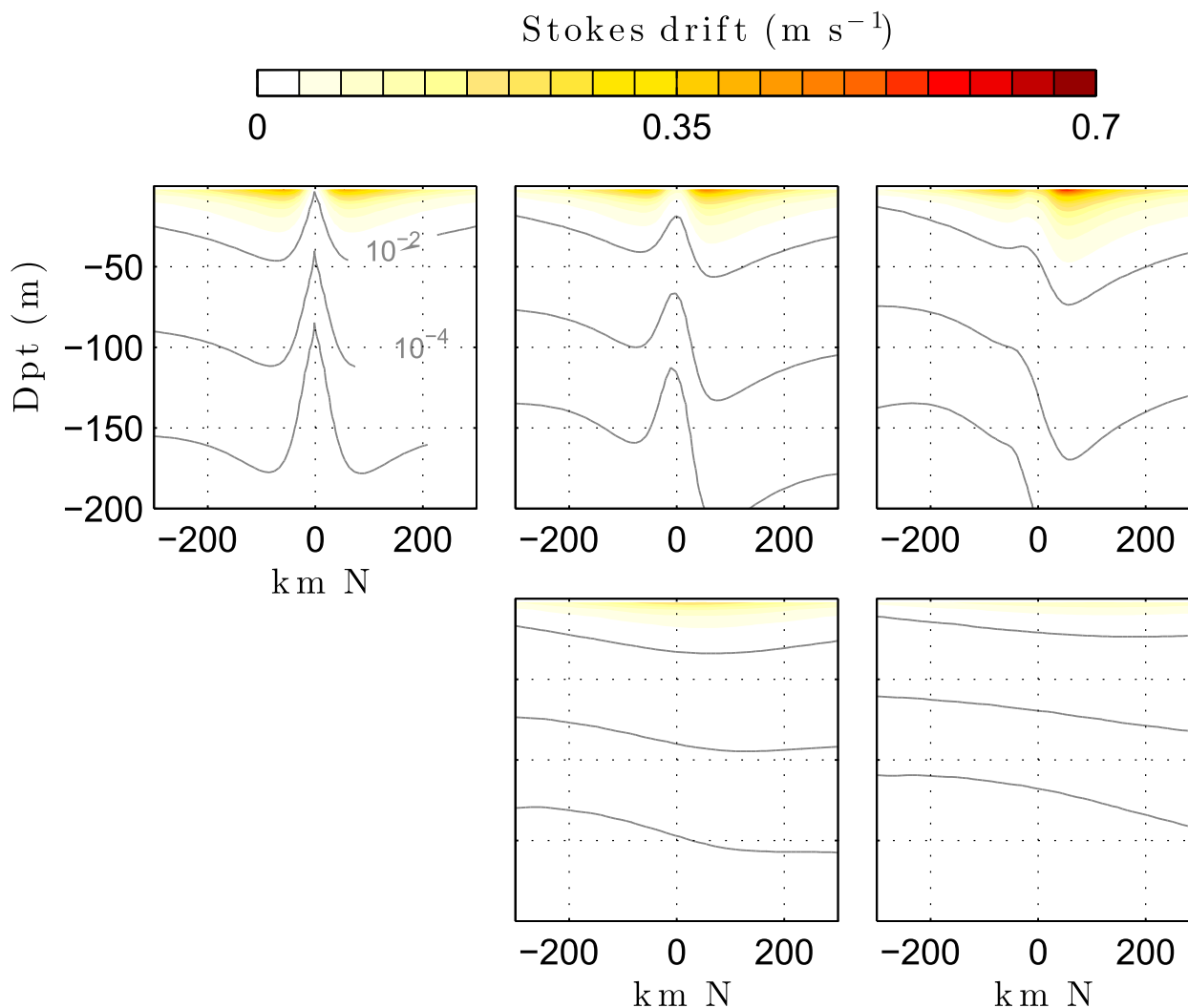
FIG. 8. As in Fig. 6, but for Stokes drift magnitude. The contours of 10^{-2}, 10^{-4}, and 10^{-6} are also included.

In KPP-ST-CS-1d (without Langmuir turbulence), the mixing layer depth peaks at 120 m on the right-hand side, compared to 70 m on the left-hand side (not shown). The mixing layer depth continues to increase on the right for a few hours after the peak wind forcing occurs, because the surface current continues to increase due to resonance between wind forcing and the inertial current response. This maintains a high level of shear-driven turbulence in the water column throughout the storm passage. On the left, the mixing layer depth peaks much earlier, and shear-driven mixing begins to decrease prior to the onset of maximum wind. This is because the maximum current occurs in front of the storm and the current quickly reduces, which leads to lower levels of shear-driven turbulence in the water column. In KPP-LT-CS-1d (in the presence of Langmuir turbulence), however, mixing is no longer only due to the shear contribution, but continues to increase beyond the

time of maximum wind on the left due to the presence of Stokes drift. This allows the mixing layer depth in KPP-LT-CS-1d to overtake the KPP-ST-CS-1d mixing layer depth by about 14 m on the left. On the right-hand side, KPP-LT-CS-1d only increases the mixing layer depth by about 7 m from KPP-ST-CS-1d, since the shear-driven mixing alone is sufficiently strong. This means that despite the lower Langmuir number on the right, Langmuir turbulence has a larger impact on the total cooling on the left. This result is consistent with previous LES results (see Fig. 2 in RWHGK, bottom-right panel).

The difference between the top panels and middle panels of Fig. 10 shows that Langmuir turbulence significantly modifies the three-dimensional processes (upwelling and horizontal advection). To understand the three-dimensional effect, in the bottom we present the difference of the temperature between the top and the middle. Since the sum of the middle
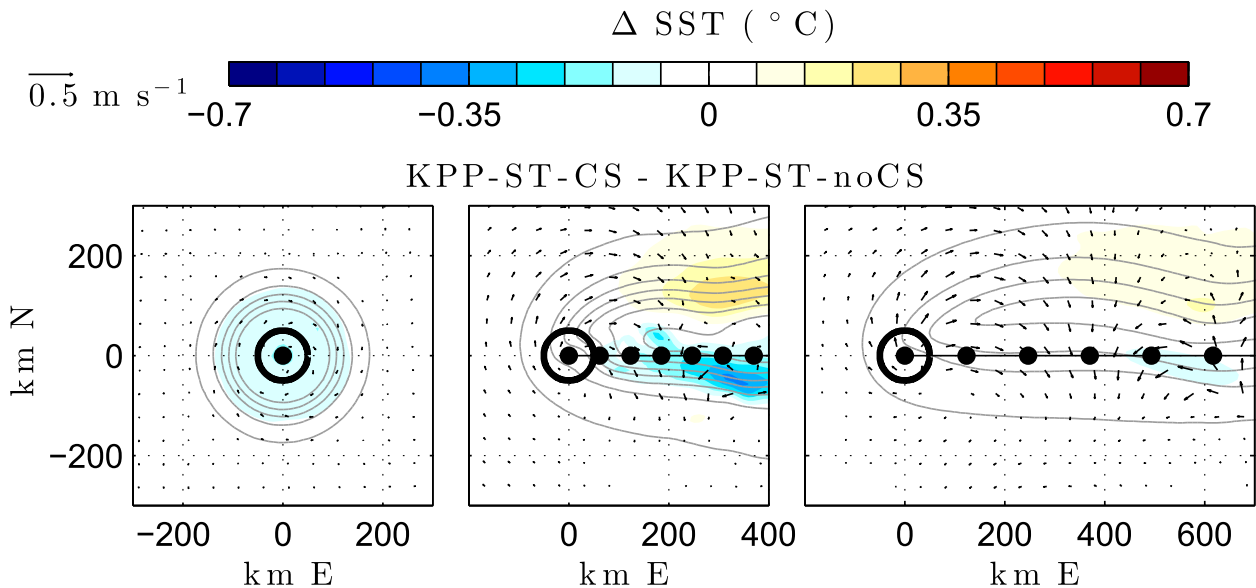
FIG. 9. Difference between KPP-ST-CS and KPP-ST-noCS for surface temperature (color map) and currents at 11.25-m depth (vectors), with the gray contours representing isotherms from KPP-ST-CS in 2°C increments for the stationary case and 1°C increments for the moving cases. The black circles represent the storm center location at 6-h increments and the thick black line represents the radius of maximum wind. The same three storms are presented as in Fig. 1.

(one-dimensional effect) and the bottom is equal to the top (total effect), the bottom panels can be interpreted as the Langmuir turbulence effect on three-dimensional processes. [This approach can equivalently be thought of as taking the difference between the three-dimensional impact with Langmuir turbulence (KPP-LT-CS − KPP-LT-CS-1d) and the three-dimensional impact with shear-only turbulence (KPP-ST-CS − KPP-ST-CS-1d).] This interpretation is valid if the one-dimensional effect and the three-dimensional effect are not strongly (non-linearly) coupled. We superimpose the vector current difference and the background temperature field (isotherms) from the KPP-LT-CS simulation in the bottom panels (both are copied from the top panels) to show the impact of upwelling and horizontal advection.

With the stationary storm (bottom-left panel), the Langmuir turbulence raises the surface temperature by over 0.7°C around the radius of maximum wind. This is due to a large reduction of the upwelling due to the decreased divergent horizontal current. This three-dimensional effect (reduction of upwelling) in the bottom-left panel nearly cancels the one-dimensional effect (increase of vertical mixing) in the middle-left panel and the resulting total impact is relatively small (top-left panel).

For the $2.85\,\mathrm{m\,s^{-1}}$ case, the impact of the Langmuir turbulence in the three-dimensional case is to raise the temperature on the right side of the cold wake by about 0.2°C, while it cools the temperature on the left-side of the cold wake by about 0.2°C. These temperature differences in the three-dimensional case appear because the reduced current due to Langmuir turbulence reduces horizontal advection of the cold wake. As in the case of the CS force, the reduction of the current (vector current difference) is directed inward toward the cold wake on the right, warming the surface temperature, and is directed outward away from the cold wake on the left, cooling the surface temperature. For the $5.7\,\mathrm{m\,s^{-1}}$ case the advection effect is reduced.

In conclusion, the Langmuir turbulence impacts are summarized as follows. First, Langmuir turbulence always enhances the vertical mixing, the mixed layer deepening, and the resulting SST cooling. Although the intensity of Langmuir turbulence is determined by the turbulent Langmuir number, its impact on the sea surface cooling is more complex, depending on the local mixing layer depth. Second, Langmuir turbulence decreases the current magnitude inside the mixing layer (because of the enhanced vertical momentum mixing). Hence, it modifies the horizontal heat advection pattern and the resulting cold-wake spatial structure. It also weakens the upwelling due to the horizontal current divergence and reduces the resulting sea surface cooling for stationary and slow-moving storms.

e. Explicit versus implicit Langmuir turbulence model

Section 3d focused on the Langmuir turbulence effects compared to the shear-only mixing results. Here, a more practical question is addressed: How well can an
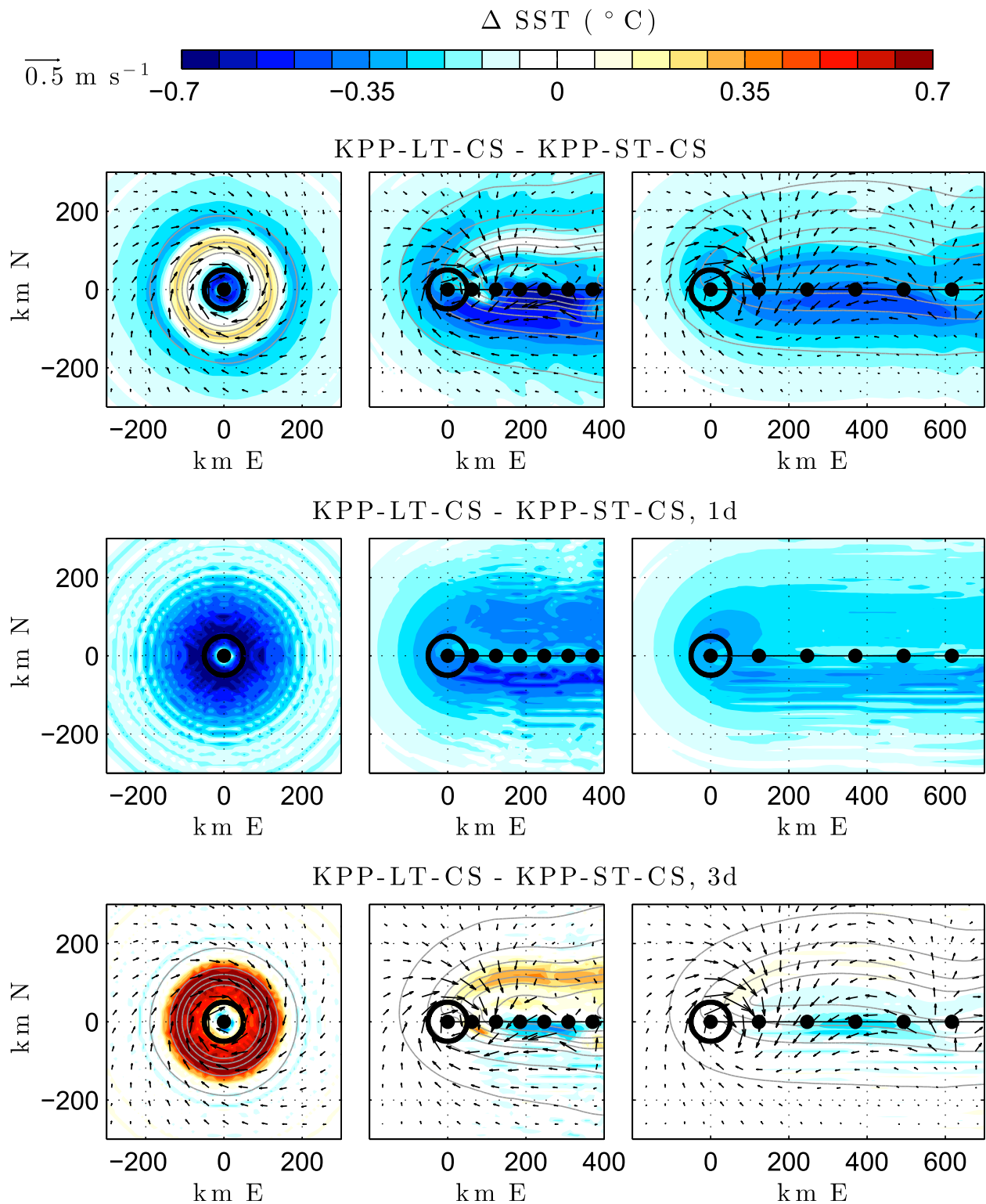
FIG. 10. (top) The difference between KPP-LT-CS and KPP-ST-CS for surface temperature (color map) and currents at 11.25-m depth (vectors), with the gray contours representing isotherms from KPP-LT-CS in 2°C increments for the stationary case and 1°C increments for the moving cases. (middle) The surface temperature difference between KPP-LT-CS-1d and KPP-ST-CS-1d. (bottom) The difference between (top) and (middle) for surface temperature, with the same arrows and gray contours as in (top). The black circles represent the storm center location at 6-h increments and the thick black line represents the radius of maximum wind. The same three storms are presented as in Fig. 1.

implicit Langmuir turbulence scheme commonly used in ocean circulation models perform relative to an explicit scheme? As discussed earlier, the mean Langmuir turbulence impacts can be included in an implicit manner by tuning the critical Richardson number used in the KPP [KPP-iLT, see section 2a(1)]. The computational requirements of a surface wave model are not nominal, so the explicit Langmuir turbulence scheme is more costly to employ. Therefore, we aim to determine whether the explicit scheme improves the hurricane upper-ocean simulations significantly enough to justify such an effort.

We now repeat the same numerical experiments using KPP-iLT instead of KPP-LT. (The results are denoted KPP-iLT-CS.) In Fig. 11 the same set of plots are produced as in Fig. 10 but using KPP-iLT. The top panels of Fig. 11 show the difference of the surface temperature and the current (11.25-m depth) between KPP-iLT-CS and KPP-ST-CS. It is apparent that these results are significantly different from the top panels of Fig. 10. For the moving storms KPP-iLT-CS significantly underestimates the sea surface cooling, particularly on the left-hand side of the storm. For the stationary storm both warming and cooling are underestimated with KPP-iLT-CS.

We now focus on the middle panels of Fig. 11, which show the effect of the implicit Langmuir turbulence parameterization on the one-dimensional process (difference between KPP-iLT-CS-1d and KPP-ST-CS-1d). Again the difference of these results from the middle panels of Fig. 10 is striking. In the moving tropical cyclone cases the Langmuir turbulence effect with KPP-iLT-CS is remarkably simple; the Langmuir turbulence simply enhances the cooling in proportion to the cooling with the shear-driven turbulence only. The spatial patterns of the enhanced cooling (middle-center and middle-right panels of Fig. 11) are very similar to those of the cooling due to the shear-driven turbulence only (top-middle and top-right panels of Fig. 2). This simple response is not surprising because the KPP-iLT scheme just modifies the critical Richardson number compared to the KPP-ST scheme. This is in stark contrast to the rather complex Langmuir turbulence effect with KPP-LT as explained earlier.

The cooling is also reduced in the stationary case with KPP-iLT-CS-1d (middle-left panel of Fig. 11) compared to KPP-ST-CS-1d (middle-left panel of Fig. 10). This difference is due to a similar reason as on the left-hand side of the moving storms. The Langmuir turbulence effect is weak with KPP-iLT-CS-1d because the current is weak and vertical mixing is not as strong with the KPP-ST scheme. The Langmuir turbulence effect is stronger with KPP-LT-CS-1d because the shear-driven

turbulence is weak and even a small enhancement of vertical mixing due to the Stokes drift makes a large impact.

As in Fig. 10, we can take the difference between the top and the middle panels to approximate the Langmuir turbulence modification to the horizontal advection and the upwelling (bottom of Fig. 11). The huge difference between KPP-iLT-CS (bottom-left panel of Fig. 11) and KPP-LT-CS (bottom-left panel of Fig. 10) for the stationary storm case can be explained as follows. As discussed earlier, KPP-LT significantly reduces and homogenizes the current magnitude inside the mixing layer because of the enhanced vertical momentum mixing (Fig. 7). KPP-iLT hardly modifies the current magnitude. This is clearly seen in Fig. 12, where the vertical transect of the current magnitude is shown. The results in Fig. 12 are almost identical to the results of the shear only case (KPP-ST-noCS) in Fig. 4 rather than the results of KPP-LT-CS in Fig. 7. Because KPP-iLT-CS does not reduce the current, it does not appreciably reduce the horizontal current divergence and the resulting upwelling, as seen in the bottom-left panel of Fig. 11. This is in contrast to the significant reduction of the upwelling effect (i.e., warming) in the bottom-left panel of Fig. 10. Because of the reduced current modification by KPP-iLT-CS, the horizontal advection effects in the moving storm cases are also reduced/modified (bottom-middle and bottom-right panels of Fig. 11) compared to the KPP-LT-CS results (bottom-middle and bottom-right panels of Fig. 10).

Finally, we investigate the difference between the explicit and implicit parameterizations by directly comparing KPP-LT-CS and KPP-iLT-CS in Fig. 13. The top panels indeed confirm that KPP-iLT-CS significantly underestimates the cooling (particularly on the left side of the moving storm) and underestimates the current magnitude reduction (i.e., overestimates the current magnitude). The difference between KPP-LT-CS and KPP-iLT-CS in Fig. 13 (top panels) is not significantly smaller than the difference between KPP-LT-CS and KPP-ST-CS in Fig. 10 (top panels). This suggests that the implicit parameterization (KPP-iLT) is not very skillful in predicting the overall the Langmuir turbulence effect on the upper-ocean response under a tropical storm, compared to the explicit parameterization (KPP-LT).

4. Discussion

As discussed earlier, the most significant feedback mechanism from the upper ocean to the tropical cyclone is through changes in the SST and the resulting surface latent heat flux. We have demonstrated that the SST cooling is significantly modified by the surface-wave-induced
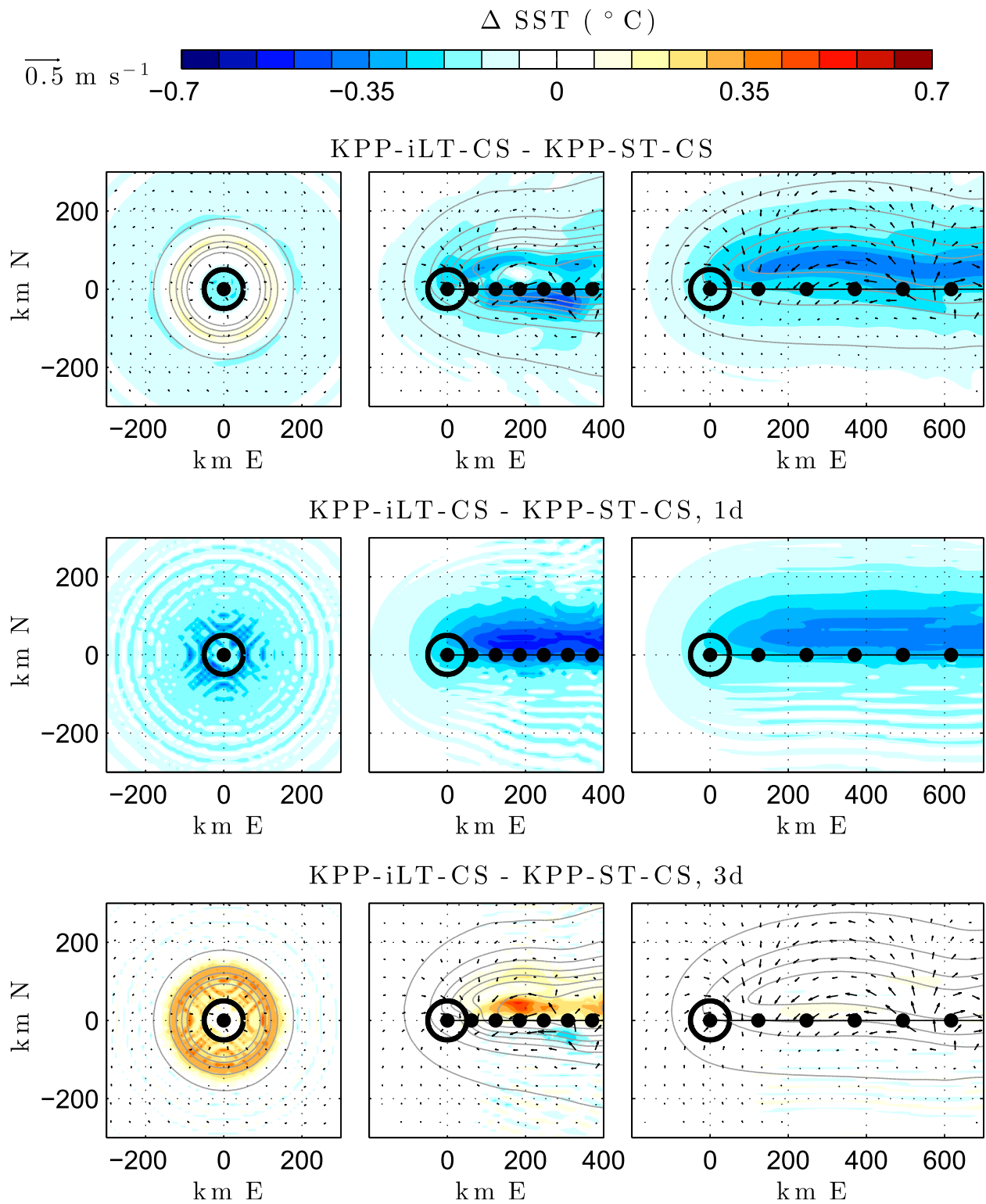
FIG. 11. As in Fig. 10, but with KPP-iLT-CS instead of KPP-LT-CS and with KPP-iLT-CS-1d instead of KPP-LT-CS-1d.
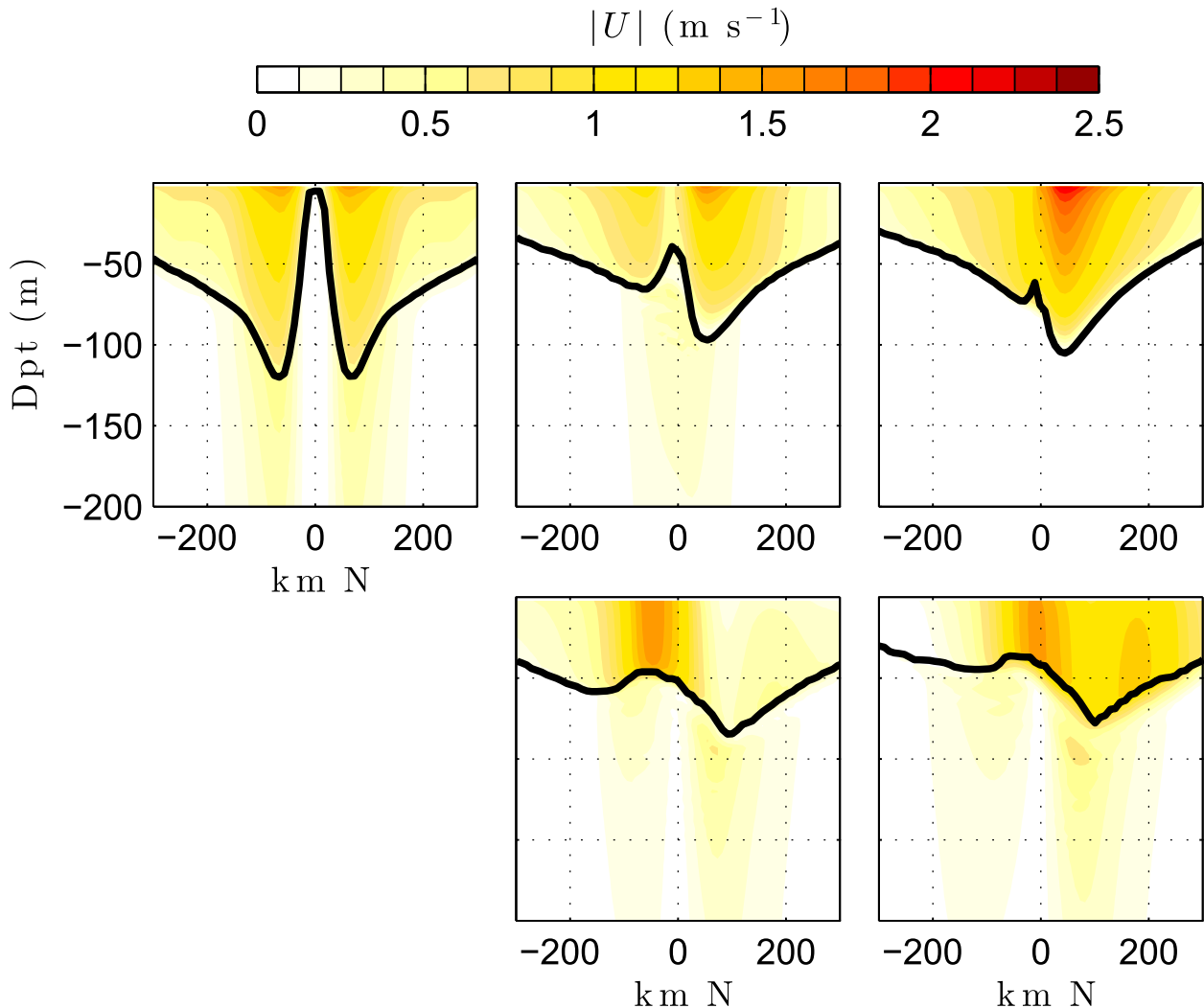
$|U| \ (\mathrm{m \ s^{-1}})$

FIG. 12. As in Fig. 4, but with KPP-iLT-CS instead of KPP-LT-CS.

Langmuir turbulence. Since this study specifies wind forcing fields and does not allow the feedback from the upper ocean to the tropical storm, it is difficult to estimate the impact of the Langmuir turbulence on the heat flux, since the near-surface air temperature and humidity are modified in response to the changes in the SST in a real storm. Nevertheless, estimates can be made of the impact on the heat flux if the near-surface air temperature and humidity are specified and assumed unaffected by the sea surface cooling. For example, using an air temperature of 23°C and a humidity of 95% (comparable to values used in previous literature), the reduction of the heat flux can be greater than 50 W m^{-2} (roughly 10% of the total heat flux) in some locations comparing the KPP-LT and KPP-iLT. We certainly expect that this large modification of the heat flux would have a significant impact on the tropical cyclone evolution.

We have so far investigated the Langmuir turbulence effect using a storm with one size and one intensity, and with one initial ocean temperature profile. We have also examined the sensitivity of the results to different storm sizes, storm intensities, translation velocities, and different initial ocean profiles. In general, the Langmuir turbulence effect is more significant if the storm is larger and more intense, due to the increased waves (Stokes drift). The Langmuir turbulence effect on SST is also stronger if the initial mixed layer is shallower and if the temperature gradient below the mixed layer is larger. For example, the Langmuir turbulence is more significant with the typical temperature profile in the Gulf of Mexico compared to the typical profile in the Caribbean Sea with a larger mixed layer depth.

We have found that the depth-averaged Eulerian current significantly exceeds the depth-averaged Stokes

Δ SST ($^\circ$C)

$\overrightarrow{0.5}$ m s^{-1} −0.7   −0.35   0   0.35   0.7
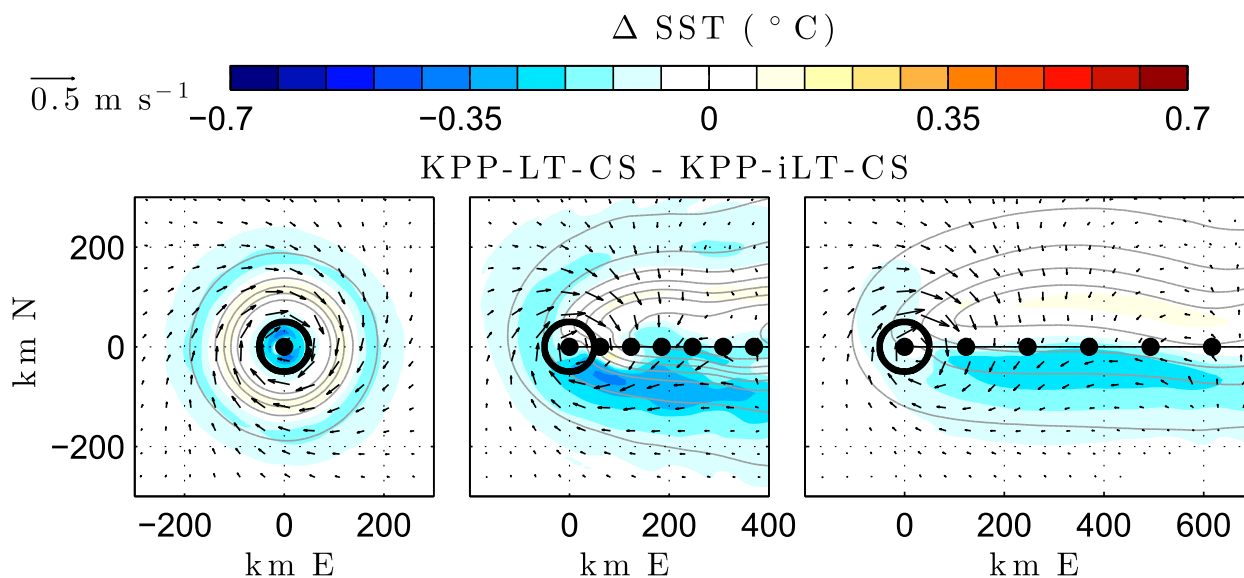
KPP-LT-CS - KPP-iLT-CS

FIG. 13. Difference between KPP-LT-CS and KPP-iLT-CS for surface temperature (color map) and currents at 11.25-m depth (vectors), with the gray contours representing isotherms from KPP-LT-CS in 2°C increments for the stationary case and 1°C increments for the moving cases. The black circles represent the storm center location at 6-h increments and the thick black line represents the radius of maximum wind. The same three storms are presented as in Fig. 1.

drift, at least in tropical cyclone conditions, indicating that advection due to Eulerian currents is more important than that due to Stokes drift (cf. Figs. 7 and 8). However, the magnitude of the Stokes drift can be comparable to the magnitude of the Eulerian current very near the surface. To further investigate the importance of Stokes drift advection, we have conducted an identical set of simulations where the mixing occurred down the gradient of the Eulerian current rather than the Lagrangian current (but including the Langmuir turbulence enhancements to the mixing coefficient and the unresolved turbulent shear component of the bulk Richardson number). This experiment results in a near-surface Eulerian current that is very similar to the Lagrangian current in the original case. We have found that the results from the case with the Eulerian mixing only and the experiment with the additional explicit Stokes drift mixing are nearly identical, suggesting the Stokes drift component to the advection is indeed small when the Eulerian component is as strong as it is under tropical cyclones.

In this study we have focused on the impacts of the Langmuir turbulence and the Coriolis–Stokes force, and have not incorporated the other wave impacts (i.e., the Stokes vortex force, the Stokes advection, and the air–sea momentum flux budget). Our results suggest that the Langmuir turbulence has the leading order wave impact on the upper-ocean response to tropical cyclones and all the other wave impacts are smaller. Nevertheless, it is known that it is dynamically inconsistent to include the

Stokes–Coriolis force in a situation where advection by the currents is important without also including the advective vortex force in the momentum and Stokes advection in material concentration equations. It is, therefore, highly desirable to extend this study to include and assess all the wave impacts in future efforts.

5. Conclusions

We have explored the modification of the ocean response to tropical cyclones due to Langmuir turbulence and the Coriolis–Stokes force. The Coriolis–Stokes force increases the upwelling in a slowly moving tropical storm, contributing to the total cooling in the storm's cold wake. It also modifies the horizontal advection of the cold wake by the storm-induced current. However, the impact of the Coriolis–Stokes force is much weaker than the impact of Langmuir turbulence.

Next, we investigated the impact of the explicit Langmuir turbulence parameterization compared to the turbulent mixing parameterization that accounts only for shear-induced turbulence. Langmuir turbulence always enhances the vertical mixing, the mixed layer deepening, and the sea surface cooling. It also reduces and homogenizes currents inside the mixing layer because of the enhanced vertical momentum mixing. Although the intensity of Langmuir turbulence is determined by the turbulent Langmuir number, its impact on the sea surface cooling is more complex, depending on the local mixing layer depth. The

reduction of the horizontal currents significantly modifies the horizontal advection of heat and reduces the cooling due to upwelling for stationary and slow-moving storms.

We have also compared the impacts of the explicit (sea-state dependent) and implicit (independent of sea states) Langmuir turbulence parameterizations. Although the implicit parameterization also introduces some enhanced SST cooling, it significantly underestimates the cooling, particularly on the left of a propagating storm, and overestimates the currents. The implicit scheme not only misses the impact of sea-state dependence on the surface cooling, but it also misrepresents the impact of the Langmuir turbulence on the Eulerian advection. Therefore, we have confirmed that the implicit scheme does not adequately represent the Langmuir turbulence effects in realistic, three-dimensional simulations of the upper-ocean response to a tropical storm.

The next step of this research is to include the explicit Langmuir turbulence parameterization (KPP-LT) in a fully coupled hurricane–wave–ocean system and to investigate the feedback of the modified SST to the storm evolution. This study suggests that explicitly resolving the sea-state-dependent Langmuir turbulence will lead to increased accuracy in predicting the air–sea fluxes and thus the intensity and track forecasts of tropical cyclones.

REFERENCES

Bender, M. A., and I. Ginis, 2000: Real-case simulations of hurricane–ocean interaction using a high-resolution coupled model: Effects on hurricane intensity. *Mon. Wea. Rev.*, **128**, 917–946, doi:10.1175/1520-0493(2000)128<0917:RCSOHO>2.0.CO;2.

Blumberg, A. F., and G. L. Mellor, 1987: A description of a three-dimensional coastal ocean circulation model. *Three-Dimensional Coastal Ocean Models*, N. S. Heaps, Ed., Vol. 4, Amer. Geophys.Union, 1–16, doi:10.1029/CO004p0001.

Craik, A. D. D., and S. Leibovich, 1976: A rational model for Langmuir circulations. *J. Fluid Mech.*, **73**, 401–426, doi:10.1017/S0022112076001420.

Emanuel, K. A., 1991: The theory of hurricanes. *Annu. Rev. Fluid Mech.*, **23**, 179–196, doi:10.1146/annurev.fl.23.010191.001143.

——, 1999: Thermodynamic control of hurricane intensity. *Nature*, **401**, 665–669, doi:10.1038/44326.

Fan, Y., and S. M. Griffies, 2014: Impacts of parameterized Langmuir turbulence and nonbreaking wave mixing in global climate simulations. *J. Climate*, **27**, 4752–4775, doi:10.1175/JCLI-D-13-00583.1.

——, I. Ginis, T. Hara, C. W. Wright, and E. J. Walsh, 2009: Numerical simulations and observations of surface wave fields under an extreme tropical cyclone. *J. Phys. Oceanogr.*, **39**, 2097–2116, doi:10.1175/2009JPO4224.1.

——, ——, and ——, 2010: Momentum flux budget across the air–sea interface under uniform and tropical cyclone winds. *J. Phys. Oceanogr.*, **40**, 2221–2242, doi:10.1175/2010JPO4299.1.

Ginis, I., 2002: Tropical cyclone–ocean interactions. *Atmosphere–Ocean Interactions*, W. Perrie, Ed., Advances in Fluid Mechanics Series, Vol. 1, WIT Press, 83–114.

Harcourt, R. R., 2013: A second-moment closure model of Langmuir turbulence. *J. Phys. Oceanogr.*, **43**, 673–697, doi:10.1175/JPO-D-12-0105.1.

——, 2015: An improved second-moment closure model of Langmuir turbulence. *J. Phys. Oceanogr.*, **45**, 84–103, doi:10.1175/JPO-D-14-0046.1.

——, and E. A. D'Asaro, 2008: Large-eddy simulation of Langmuir turbulence in pure wind seas. *J. Phys. Oceanogr.*, **38**, 1542–1562, doi:10.1175/2007JPO3842.1.

Hasselmann, K., 1970: Wave-driven intertial oscillations. *Geophys. Fluid Dyn.*, **1**, 463–502, doi:10.1080/03091927009365783.

Holland, G. J., 1980: An analytic model of the wind and pressure profiles in hurricanes. *Mon. Wea. Rev.*, **108**, 1212–1218, doi:10.1175/1520-0493(1980)108<1212:AAMOTW>2.0.CO;2.

Kantha, L. H., and C. A. Clayson, 2004: On the effect of surface gravity waves on mixing in the oceanic mixed layer. *Ocean Modell.*, **6**, 101–124, doi:10.1016/S1463-5003(02)00062-8.

Kukulka, T., A. J. Plueddemann, J. H. Trowbridge, and P. P. Sullivan, 2009: Significance of Langmuir circulation in upper ocean mixing: Comparison of observations and simulations. *Geophys. Res. Lett.*, **36**, L10603, doi:10.1029/2009GL037620.

Large, W. G., J. C. McWilliams, and S. C. Doney, 1994: Oceanic vertical mixing: A review and a model with a nonlocal boundary layer parameterization. *Rev. Geophys.*, **32**, 363–403, doi:10.1029/94RG01872.

Li, Q., A. Webb, B. Fox-Kemper, A. Craig, G. Danabasoglu, W. G. Large, and M. Vertenstein, 2016: Langmuir mixing effects on global climate: WAVEWATCH III in CESM. *Ocean Modell.*, **103**, 145–160, doi:10.1016/j.ocemod.2015.07.020.

McWilliams, J. C., and J. M. Restrepo, 1999: The wave-driven ocean circulation. *J. Phys. Oceanogr.*, **29**, 2523–2540, doi:10.1175/1520-0485(1999)029<2523:TWDOC>2.0.CO;2.

——, and P. P. Sullivan, 2000: Vertical mixing by Langmuir circulations. *Spill Sci. Technol. Bull.*, **6**, 225–237, doi:10.1016/S1353-2561(01)00041-X.

——, ——, and C.-H. Moeng, 1997: Langmuir turbulence in the ocean. *J. Fluid Mech.*, **334**, 1–30, doi:10.1017/S0022112096004375.

——, E. Huckle, J.-H. Liang, and P. P. Sullivan, 2012: The wavy Ekman layer: Langmuir circulations, breaking waves, and Reynolds stress. *J. Phys. Oceanogr.*, **42**, 1793–1816, doi:10.1175/JPO-D-12-07.1.

Mellor, G. L., 2004: User's guide for a three-dimensional, primitive equation, numerical ocean model. Tech. Rep., Program in Atmospheric and Oceanic Science, Princeton University, 56 pp. [Available online at http://jes.apl.washington.edu/modsims_two/usersguide0604.pdf.]

——, and T. Yamada, 1974: A hierarchy of turbulence closure models for planetary boundary layers. *J. Atmos. Sci.*, **31**, 1791–1806, doi:10.1175/1520-0469(1974)031<1791:AHOTCM>2.0.CO;2.

——, and ——, 1982: Development of a turbulence closure model for geophysical fluid problems. *Rev. Geophys. Space Phys.*, **20**, 851–875, doi:10.1029/RG020i004p00851.

Moon, I.-J., I. Ginis, and T. Hara, 2008: Impact of the reduced drag coefficient on ocean wave modeling under hurricane conditions. *Mon. Wea. Rev.*, **136**, 1217–1223, doi:10.1175/2007MWR2131.1.

Noh, Y., H. S. Min, and S. Raasch, 2004: Large eddy simulation of the ocean mixed layer: The effects of wave breaking and

Langmuir circulation. *J. Phys. Oceanogr.*, **34**, 720–735, doi:10.1175/1520-0485(2004)034<0720:LESOTO>2.0.CO;2.

Polton, J. A., and S. E. Belcher, 2007: Langmuir turbulence and deeply penetrating jets in an unstratified mixed layer. *J. Geophys. Res.*, **112**, C09020, doi:10.1029/2007JC004205.

——, D. M. Lewis, and S. E. Belcher, 2005: The role of wave-induced Coriolis–Stokes forcing on the wind-driven mixed layer. *J. Phys. Oceanogr.*, **35**, 444–457, doi:10.1175/JPO2701.1.

Price, J. F., 1981: Upper ocean response to a hurricane. *J. Phys. Oceanogr.*, **11**, 153–175, doi:10.1175/1520-0485(1981)011<0153:UORTAH>2.0.CO;2.

Rabe, T. J., T. Kukulka, I. Ginis, T. Hara, B. G. Reichl, E. A. D'Asaro, R. R. Harcourt, and P. P. Sullivan, 2015: Langmuir turbulence under Hurricane Gustav (2008). *J. Phys. Oceanogr.*, **45**, 657–677, doi:10.1175/JPO-D-14-0030.1.

Reichl, B. G., D. Wang, T. Hara, I. Ginis, and T. Kukulka, 2016: Langmuir turbulence parameterization in tropical cyclone conditions. *J. Phys. Oceanogr.*, **46**, 863–886, doi:10.1175/JPO-D-15-0106.1.

Smyth, W. D., E. D. Skyllingstad, G. B. Crawford, and H. Wijesekera, 2002: Nonlocal fluxes and Stokes drift effects in the K-Profile Parameterization. *Ocean Dyn.*, **52**, 104–115, doi:10.1007/s10236-002-0012-9.

Sullivan, P. P., L. Romero, J. C. McWilliams, and W. K. Melville, 2012: Transient evolution of Langmuir turbulence in ocean boundary layers driven by hurricane winds and waves. *J. Phys. Oceanogr.*, **42**, 1959–1980, doi:10.1175/JPO-D-12-025.1.

Tolman, H. L., 2009: User manual and system documentation of WAVEWATCH III version 3.14. Tech. Note 276, NOAA/NWS/NCEP/EMC/MMAB, 194 pp.

Umlauf, L., H. Burchard, and K. Bolding, 2005: GOTM: Source-code and test case documentation, version 4.0. 3rd ed. Leiniz-Institute for Baltic Sea Research Marine Science, 360 pp. [Available online at http://www.gotm.net/pages/documentation/manual/stable/pdf/a4.pdf.]

Ursell, F., and G. E. R. Deacon, 1950: On the theoretical form of ocean swell on a rotating earth. *Geophys. J. Int.*, **6** (Suppl.), 1–8, doi:10.1111/j.1365-246X.1950.tb02968.x.

Van Roekel, L. P., B. Fox-Kemper, P. P. Sullivan, P. E. Hamlington, and S. R. Haney, 2012: The form and orientation of Langmuir cells for misalinged winds and waves. *J. Geophys. Res.*, **117**, C05001, doi:10.1029/2011JC007516.

Vincent, E. M., M. Lengaigne, J. Vialard, G. Madec, N. C. Jourdain, and S. Masson, 2012: Assessing the oceanic control on the amplitude of sea surface cooling induced by tropical cyclones. *J. Geophys. Res.*, **117**, C05023, doi:10.1029/2011JC007705.

Yablonsky, R. M., and I. Ginis, 2009: Limitation of one-dimensional ocean models for coupled hurricane–ocean model forecasts. *Mon. Wea. Rev.*, **137**, 4410–4419, doi:10.1175/2009MWR2863.1.

——, and B. Thomas, 2015a: Ocean modeling with flexibile initialization for improved coupled tropical cyclone–ocean model prediction. *Environ. Modell. Software*, **67**, 26–30, doi:10.1016/j.envsoft.2015.01.003.

——, ——, ——, V. Tallapragada, D. Sheinin, and L. Bernardet, 2015b: Description and analysis of the ocean component of NOAA's operational Hurricane Weather Research and Forecasting (HWRF) Model. *J. Atmos. Oceanic Technol.*, **32**, 144–163, doi:10.1175/JTECH-D-14-00063.1.